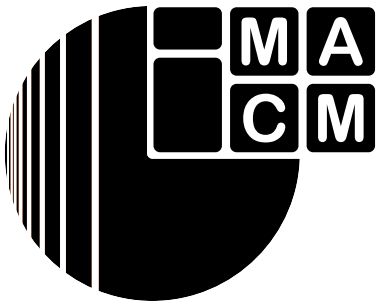

Bergische Universität Wuppertal

Fachbereich Mathematik und Naturwissenschaften

Institute of Mathematical Modelling, Analysis and Computational Mathematics (IMACM)

Preprint BUW-IMACM 11/16

Andreas Bartel, Markus Brunk, Michael Günther, Sebastian Schöps

Dynamic Iteration for Coupled Problems of Electric Circuits and Distributed Devices

September 2011

http://www.math.uni-wuppertal.de

DYNAMIC ITERATION FOR COUPLED PROBLEMS OF ELECTRIC CIRCUITS AND DISTRIBUTED DEVICES*

ANDREAS BARTEL, MARKUS BRUNK, MICHAEL GÜNTHER, SEBASTIAN SCHÖPS†

Abstract. Coupled systems of differential-algebraic equations (DAEs) may suffer from instabilities during a dynamic iteration. For a general dynamic iteration, we extend the existing analysis on recursion estimates, error transport and stability to a general DAE setting. In this context, we discuss the influence of certain coupling structures and the computational sequence of the subsystems on the rate of convergence. Furthermore, we investigate convergence and divergence for two coupled problems stemming from refined electric circuit simulation in detail. These are the semiconductor-circuit and field-circuit coupling. As a result of our analysis, we quantify the convergence rate and behavior also using Lipschitz constants and suggest an enhanced modeling of the coupling interface in order to improve convergence.

Key words. Dynamic Iteration, Co-Simulation, Mixed Mode Simulation, PDAE, Coupling, Electric circuit simulation.

AMS subject classifications. 65L05, 65L80, 65L20.

1. Introduction. In today's applications, multiphysical modeling is indispensable due to miniaturization and the increasing complexity of components. Thus coupled simulation (or simulator coupling) is naturally needed. That is, different simulation packages are applied to different subsystems and often one cannot solve the system as a whole in the time-domain. Even if this is possible, it remains a challenging task for time-integrators: the intrinsic time rates of the subsystems can differ by several orders of magnitude and the structure of the subsystems can differ significantly, e.g. with respect to symmetry and definiteness. This holds in particular for applications from electrical engineering. When coupling an electric circuit to a distributed device (mixed mode simulation [15]), the circuit is commonly described by differential algebraic equations (DAEs) using a network approach, whereas the device is modeled by partial differential equations (PDEs). The network system is generally not symmetric and typically integrated by direct solvers, whereas the discretized PDE typically forms a symmetric system that is commonly solved by iterative methods. Standard time-integration is inefficient for those problems. One way to overcome this impasse is to revisit co-simulation, [29].

This paper addresses the (time-domain) co-simulation of PDAE systems, i.e., the time-integration of systems of PDEs and DAEs by the means of dynamic iteration. First, dynamic iteration has been applied to coupled ordinary differential equations (ODEs), where they are known to be unconditionally stable, [21, 9]. Usually a windowing technique is applied to enhance convergence, i.e., the contractivity of the related fixed-point operator. However, in the applications of dynamic iteration schemes to DAEs, severe instabilities occurred. The contraction of the fixed-point operator can only be guaranteed if a stability constraint is fulfilled. This concept dates back to Lelarasmee [18] and was applied for single window convergence [16, 5]. The error transport for multiple windows has been analyzed for DAEs with a special coupling

*The authors specially thank Giuseppe Alì for the fruitful discussions and his suggestions for the initial proof of the fixed point iteration. The authors are indebted to the ICESTARS project, which is funded by the seventh framework programme of the European Union with the grant number ICT214911 and to the SOFA project, funded by the BMBF with the grant number 03MS648E.

†Bergische Universität Wuppertal, Gaußstr. 20, 42119 Wuppertal, Germany.
Email: {bartel,guenther,schoeps}@math.uni-wuppertal.de, mail@markus-brunk.de

structure of Lagrangian type in [3]. In [12] the error transport was considered under the simplifying assumption that the DAE system can be reduced to its underlying ODE. The coupling structure and its influence on the stability of dynamic iteration was also studied in [17].

In this paper we present a generalization of these previous work by extending their rigorous analysis to the general DAE case. Guided by [3], we deduce a similar contractivity condition, which ensures convergence of dynamic iteration schemes applied to *general* index-1 DAEs. By examination of the error propagation for the windowing technique, we prove that the dynamic iteration scheme is globally convergent if stability is given. We identify certain coupling structures, where our analysis immediately guarantees a higher rate of convergence with respect to the time window size. This is of special interest for radio frequency applications, where the applied time window is usually rather small. We show that the sequence of computation of the subproblems can be crucial for convergence. Additionally, we verify that even if the iteration scheme is convergent independent of the sequence of the subsystems, the sequence can have severe influence onto the rate of convergence. In applications from electrical engineering, the different coupling structures and their influence onto convergence and the rate of convergence are investigated. For two different problems we suggest an enhanced modeling of the coupling interface (by overlapping or model parameter extraction) such that convergence is ensured and a higher rate of convergence can be achieved compared to coupling via the unmodified interface.

The paper is organized as follows. In Section 2 we introduce the notation for our coupled DAE-problems and the dynamic iteration schemes. In Section 3 we analyze the convergence and stability of the dynamic iteration schemes. We consider the error transport for both differential and algebraic components and show that global convergence (including error transport) is ensured if the splitting error remains close to the analytical solution. Finally, we show that the mutual dependency of the subsystems, i.e., coupling via differential or algebraic variables, is crucial for the convergence of the iteration scheme. To apply the theoretical results in circuit simulation, we recall the electric network model and discuss coupling strategies in Section 4. Based on this, we analyze two coupled problems. First we investigate the semiconductor-circuit problem in Section 5–7. Secondly, the field-circuit system is analyzed in Section 8–10. In both applications, we focus on the modeling of the coupling interface: we show under which conditions the convergence behaves like in a coupled ODE problem and how this can be obtained by sophisticated modeling, e.g. overlapping or extraction of model parameters, cf. [22]. Both examples numerically confirm the theoretical results about convergence and divergence. The paper finishes with conclusions.

2. Description of coupled DAE systems for dynamic iteration schemes. We address the time domain simulation of coupled problems. To this end, we assume that a suitable spatial discretization is already applied to a coupled PDAE problem and consider the time integration of the resulting coupled DAE problem. A large class of these initial value problems (IVPs) can be written in semi-explicit form:

$$\dot{\mathbf{y}} = \mathbf{f}(\mathbf{y}, \mathbf{z}), \qquad \mathbf{y}(0) = \mathbf{y}_0, \tag{2.1a}$$

$$0 = \mathbf{g}(\mathbf{y}, \mathbf{z}), \qquad \mathbf{z}(0) = \mathbf{z}_0. \tag{2.1b}$$

This formulation addresses the whole system at once, but suppresses the subsystem structuring, which will serve us to extract certain principle results and allow for condensed argumentations. Under the following assumption, $\mathbf{y}$ denotes the differential variables and $\mathbf{z}$ the algebraic variables of the system (2.1).

ASSUMPTION 2.1. *Given problem* (2.1).

a) The right-hand side functions and the initial values (IVs) are assumed to guarantee a unique solution $\mathbf{x}$ *on* $[0, t_e]$*:*

$$\mathbf{x} := (\mathbf{y}, \mathbf{z})^\top \quad \textit{with} \quad \mathbf{y} : [0, t_e] \to \mathbb{R}^{n_y},\ \mathbf{z} : [0, t_e] \to \mathbb{R}^{n_z}$$

(neglecting some transpose signs to keep the notations simple).

b) Functions $\mathbf{f}$ *and* $\mathbf{g}$ *are supposed to be sufficiently often differentiable in the neighborhood of the unique solution.*

c) The Jacobian $\partial\mathbf{g}/\partial\mathbf{z}$ *is non-singular in the neighborhood of the solution.*

Assumption 2.1 ensures consistent IVs and the system (2.1) to be of index-1.

2.1. Coupled system representation. In a multiphysical framework, system (2.1) is often naturally partitioned in a set of r coupled DAE subsystems:

$$\dot{\mathbf{y}}_i = \mathbf{f}_i(\mathbf{y}, \mathbf{z}), \qquad (\mathbf{y} = (\mathbf{y}_1, \ldots, \mathbf{y}_r)^\top) \tag{2.2a}$$

$$0 = \mathbf{g}_i(\mathbf{y}, \mathbf{z}), \qquad (\mathbf{z} = (\mathbf{z}_1, \ldots, \mathbf{z}_r)^\top) \tag{2.2b}$$

for $i = 1, \ldots, r$, and $\mathbf{f} = (\mathbf{f}_1, \ldots, \mathbf{f}_r)^\top$, $\mathbf{g} = (\mathbf{g}_1, \ldots, \mathbf{g}_r)^\top$. In order to ensure index-1 for each subsystem, in this framework, additionally to Assumption 2.1, it has to hold

$$\partial\mathbf{g}_i/\partial\mathbf{z}_i \text{ is non-singular for all } i = 1, \ldots, r, \tag{2.3}$$

i.e., each subsystem $\mathbf{g}_i(\mathbf{y}, \mathbf{z}) = 0$ is locally, uniquely solvable for $\mathbf{z}_i$ (for given $\mathbf{y}$, $\mathbf{z}_1$, $\ldots$, $\mathbf{z}_{i-1}$, $\mathbf{z}_{i+1}$, $\ldots$, $\mathbf{z}_r$).

REMARK 2.2 (Overlapping). *In some settings, certain quantities (and corresponding algebraic constraints) can be assigned to several subsystems. This is called overlapping. It introduces additional degrees of freedom to the latter dynamic iteration scheme, see e.g. [4]. Here, these aspects are not discussed.*

2.2. Iteration schemes. Starting for a general DAE (2.1), any dynamic iteration scheme needs to work on a split structure, e.g. on (2.2). This allows to exploit special structures or properties by invoking dedicated solvers. To analyze dynamic iteration methods, we formalize this procedure: we seek to compute a sufficiently accurate numerical approximation $\tilde{\mathbf{x}}$ of the unique $\mathbf{x}$ for (2.1) with

$$\tilde{\mathbf{x}} := (\tilde{\mathbf{y}}, \tilde{\mathbf{z}})^\top : [0, t_e] \to \mathbb{R}^{n_y} \times \mathbb{R}^{n_z}.$$

Usually the iteration is performed on so called windows $[t_n, t_{n+1}]$ with $0 = t_0 < t_1 < t_2 < \ldots < t_N = t_e$ and window size $H_n := t_{n+1} - t_n$. Assuming the numerical approximation is already computed on $[0, t_n]$, a dynamic iteration defines the approximations

$$(\tilde{\mathbf{y}}, \tilde{\mathbf{z}})|_{[t_n, t_{n+1}]} \in C_n^{1,0} \quad \text{with} \quad C_n^{1,0} := C^1([t_n, t_{n+1}], \mathbb{R}^{n_y}) \times C([t_n, t_{n+1}], \mathbb{R}^{n_z}),$$

on the subsequent window by an extrapolation step followed by iterations:

- *extrapolation step*: let the operator $\Phi_n : C_{n-1}^{1,0} \to C_n^{1,0}$ be a continuous extrapolation from $[t_{n-1}, t_n]$ to $[t_n, t_{n+1}]$ defining our initial guess:

$$\begin{pmatrix} \tilde{\mathbf{y}}_n^{(0)} \\ \tilde{\mathbf{z}}_n^{(0)} \end{pmatrix} := \Phi_n \begin{pmatrix} \tilde{\mathbf{y}}|_{[t_{n-1}, t_n]} \\ \tilde{\mathbf{z}}|_{[t_{n-1}, t_n]} \end{pmatrix} \qquad \text{with } \Phi_n = \begin{pmatrix} \Phi_{\mathbf{y},n} \\ \Phi_{\mathbf{z},n} \end{pmatrix}. \tag{2.4}$$

  A simple choice is a constant extrapolation, which introduces errors in $\mathcal{O}(H_n)$:

$$\tilde{\mathbf{y}}_n^{(0)}(t) = \tilde{\mathbf{y}}(t_n), \quad \mathbf{z}_n^{(0)}(t) = \tilde{\mathbf{z}}(t_n) \quad (\text{for all } t \in [t_n, t_{n+1}]).$$

  Higher order polynomials could improve this error. Such an operator satisfies a uniform Lipschitz condition independent of H_n [3].

- *iteration step*: the following iterations define a map $\Psi_n : C_n^{1,0} \to C_n^{1,0}$ as

$$\begin{pmatrix} \tilde{\mathbf{y}}_n^{(k-1)} \\ \tilde{\mathbf{z}}_n^{(k-1)} \end{pmatrix} \to \begin{pmatrix} \tilde{\mathbf{y}}_n^{(k)} \\ \tilde{\mathbf{z}}_n^{(k)} \end{pmatrix} := \Psi_n \begin{pmatrix} \tilde{\mathbf{y}}_n^{(k-1)} \\ \tilde{\mathbf{z}}_n^{(k-1)} \end{pmatrix} \qquad \text{with } \Psi_n = \begin{pmatrix} \Psi_{\mathbf{y},n} \\ \Psi_{\mathbf{z},n} \end{pmatrix} \tag{2.5}$$

with label $k = 1, \ldots, k_n$ and finite iteration number k_n. To obtain solutions to our DAE (2.1), we define Ψ_n as the solution operator for the IVP

$$\dot{\tilde{\mathbf{y}}}_n^{(k)} = \mathbf{F}(\tilde{\mathbf{y}}_n^{(k)}, \tilde{\mathbf{y}}_n^{(k-1)}, \tilde{\mathbf{z}}_n^{(k)}, \tilde{\mathbf{z}}_n^{(k-1)}) \quad \text{with IV} \quad \tilde{\mathbf{y}}_n^{(k)}(t_n) = \tilde{\mathbf{y}}_n^{(k-1)}(t_n), \tag{2.6a}$$

$$0 = \mathbf{G}(\tilde{\mathbf{y}}_n^{(k)}, \tilde{\mathbf{y}}_n^{(k-1)}, \tilde{\mathbf{z}}_n^{(k)}, \tilde{\mathbf{z}}_n^{(k-1)}). \tag{2.6b}$$

The so-called splitting functions $\mathbf{F}$ and $\mathbf{G}$ are arbitrary smooth functions, which fulfill the compatibility conditions for problem (2.1):

$$\mathbf{F}(\mathbf{y}, \mathbf{y}, \mathbf{z}, \mathbf{z}) = \mathbf{f}(\mathbf{y}, \mathbf{z}), \qquad \mathbf{G}(\mathbf{y}, \mathbf{y}, \mathbf{z}, \mathbf{z}) = \mathbf{g}(\mathbf{y}, \mathbf{z}). \tag{2.7}$$

Both $\mathbf{F}$ and $\mathbf{G}$ are assumed to be sufficiently differentiable.

REMARK 2.3. *(i) Due to compatibility* (2.7)*, the analytic solution* $\mathbf{x} := (\mathbf{y}, \mathbf{z})^\top$ *is a fixed-point of the iteration operator* Ψ_n*.*

(ii) The solution computed by dynamic iteration on $[t_n, t_{n+1}]$ *reads:*

$$\begin{pmatrix} \tilde{\mathbf{y}}|_{[t_n, t_{n+1}]} \\ \tilde{\mathbf{z}}|_{[t_n, t_{n+1}]} \end{pmatrix} = (\Psi_n^{k_n} \circ \Phi_n)(\begin{pmatrix} \tilde{\mathbf{y}}|_{[t_{n-1}, t_n]} \\ \tilde{\mathbf{z}}|_{[t_{n-1}, t_n]} \end{pmatrix}). \tag{2.8}$$

For the partition (2.2) with corresponding unknowns $\tilde{\mathbf{y}}_n = (\tilde{\mathbf{y}}_{1,n}, \ldots, \tilde{\mathbf{y}}_{r,n})^\top$, $\tilde{\mathbf{z}}_n = (\tilde{\mathbf{z}}_{1,n}, \ldots, \tilde{\mathbf{z}}_{r,n})^\top$, the iteration operator Ψ_n is defined by r initial-value problems:

$$\dot{\tilde{\mathbf{y}}}_{i,n}^{(k)} = \mathbf{F}_i(\tilde{\mathbf{y}}_n^{(k)}, \tilde{\mathbf{y}}_n^{(k-1)}, \tilde{\mathbf{z}}_n^{(k)}, \tilde{\mathbf{z}}_n^{(k-1)}), \quad \text{with} \quad \tilde{\mathbf{y}}_{i,n}^{(k)}(t_n) = \tilde{\mathbf{y}}_{i,n}^{(k-1)}(t_n), \tag{2.9a}$$

$$0 = \mathbf{G}_i(\tilde{\mathbf{y}}_n^{(k)}, \tilde{\mathbf{y}}_n^{(k-1)}, \tilde{\mathbf{z}}_n^{(k)}, \tilde{\mathbf{z}}_n^{(k-1)}) \tag{2.9b}$$

for $i = 1, \ldots, r$ and using compatible splitting functions $\mathbf{F}_i$ and $\mathbf{G}_i$, such that $\mathbf{F} = (\mathbf{F}_1, \ldots, \mathbf{F}_r)^\top$ and $\mathbf{G} = (\mathbf{G}_1, \ldots, \mathbf{G}_r)^\top$. Common dynamic iterations schemes for the coupled DAE systems (2.2) can be represented by

$$\mathbf{F}_i(\tilde{\mathbf{y}}_n^{(k)}, \tilde{\mathbf{y}}_n^{(k-1)}, \tilde{\mathbf{z}}_n^{(k)}, \tilde{\mathbf{z}}_n^{(k-1)}) = \mathbf{f}_i(\tilde{\mathbf{Y}}_{i,n}^{(k)}, \tilde{\mathbf{Z}}_{i,n}^{(k)}), \tag{2.10a}$$

$$\mathbf{G}_i(\tilde{\mathbf{y}}_n^{(k)}, \tilde{\mathbf{y}}_n^{(k-1)}, \tilde{\mathbf{z}}_n^{(k)}, \tilde{\mathbf{z}}_n^{(k-1)}) = \mathbf{g}_i(\tilde{\mathbf{Y}}_{i,n}^{(k)}, \tilde{\mathbf{Z}}_{i,n}^{(k)}) \tag{2.10b}$$

$(i = 1, \ldots, r)$. Important examples are stated in Table 2.1. In these methods, obviously, $\mathbf{F}$ and $\mathbf{G}$ inherit the differentiability from $\mathbf{f}$ and $\mathbf{g}$.

For coupled ODEs, the above discussed methods can be made convergent by choosing the window sizes sufficiently small. For DAEs an additional contractivity must be satisfied to obtain (a) the convergence of iterations within a window and (b) the stable error propagation in algebraic variables (window to window).

Table 2.1: Common dynamic iterations.

Picard:	$\tilde{\mathbf{Y}}_{i,n}^{(k)} = \tilde{\mathbf{y}}_n^{(k-1)}, \qquad \tilde{\mathbf{Z}}_{i,n}^{(k)} = \tilde{\mathbf{z}}_n^{(k-1)}.$
Jacobi:	$\tilde{\mathbf{Y}}_{i,n}^{(k)} = (\tilde{\mathbf{y}}_{1,n}^{(k-1)}, \ldots, \tilde{\mathbf{y}}_{i-1,n}^{(k-1)}, \tilde{\mathbf{y}}_{i,n}^{(k)}, \tilde{\mathbf{y}}_{i+1,n}^{(k-1)}, \ldots, \tilde{\mathbf{y}}_{r,n}^{(k-1)})^\top.$ $\tilde{\mathbf{Z}}_{i,n}^{(k)} = (\tilde{\mathbf{z}}_{1,n}^{(k-1)}, \ldots, \tilde{\mathbf{z}}_{i-1,n}^{(k-1)}, \tilde{\mathbf{z}}_{i,n}^{(k)}, \tilde{\mathbf{z}}_{i+1,n}^{(k-1)}, \ldots, \tilde{\mathbf{z}}_{r,n}^{(k-1)})^\top,$
Gauss-Seidel:	$\tilde{\mathbf{Y}}_{i,n}^{(k)} = (\tilde{\mathbf{y}}_{1,n}^{(k)}, \ldots, \tilde{\mathbf{y}}_{i,n}^{(k)}, \tilde{\mathbf{y}}_{i+1,n}^{(k-1)}, \ldots, \tilde{\mathbf{y}}_{r,n}^{(k-1)})^\top,$ $\tilde{\mathbf{Z}}_{i,n}^{(k)} = (\tilde{\mathbf{z}}_{1,n}^{(k)}, \ldots, \tilde{\mathbf{z}}_{i,n}^{(k)}, \tilde{\mathbf{z}}_{i+1,n}^{(k-1)}, \ldots, \tilde{\mathbf{z}}_{r,n}^{(k-1)})^\top.$

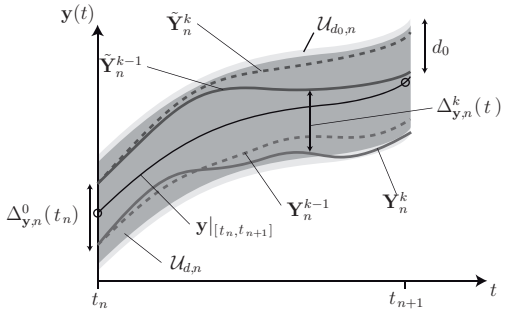

Figure 3.1: A differential waveform is shown for the k-th iteration of the time window $[t_n,\ t_{n+1}]$. The old waveforms $\tilde{\mathbf{Y}}_n^{k-1}$ and $\mathbf{Y}_n^{k-1}$ are in the smaller neighborhood $\mathcal{U}_{d,n}$, whereas the new waveforms $\tilde{\mathbf{Y}}_n^k$ and $\mathbf{Y}_n^k$ are in the larger one $\mathcal{U}_{d_0,n}$.

3. Analysis of convergence and stability. The convergence of our dynamic iteration schemes is investigated by studying error recursions within one window and the error transport from window to window. We neglect errors from time integration, i.e., we iterate on analytic waveforms. Our strategy generalizes the approach of [3] as already started in [5]. In the first part, we define the corresponding function space and deduce the error recursion on one window by tracking the constants in our estimates. Then, in the second part, we summarize the line of arguments towards contraction, general convergence and stability. In the last part, we investigate the implications of our results for the rate of convergence given certain coupling structures.

3.1. Error recursion on one window. Given $d_0 > 0$, we define for all d with $0 < d \leq d_0$ the function space $\mathcal{U}_{d,n}$ as neighborhood of the exact solution $\mathbf{x} := (\mathbf{y}, \mathbf{z})^\top$

$$\mathcal{U}_{d,n} = \left\{ \mathbf{X} := (\mathbf{Y}, \mathbf{Z})^\top \in C_n^{1,0} : \left|\left|\mathbf{Y} - \mathbf{y}|_{[t_n,t_{n+1}]}\right|\right|, \left|\left|\mathbf{Z} - \mathbf{z}|_{[t_n,t_{n+1}]}\right|\right| \leq d \right\}$$

on the $n-$th window by employing $||\mathbf{v}|| := \max_t |\mathbf{v}(t)|$ the maximum-norm in the time domain of $\mathbf{v}$ (for t from a given interval) and the Euclidean norm $|\cdot|$. The purpose of d_0 is to identify a largest function space $\mathcal{U}_{d_0,n}$ to be considered in the proofs below. In particular, the following prerequisites are considered on this function space:

ASSUMPTION 3.1. *For* (2.1) *with splitting functions* $\mathbf{F}$, $\mathbf{G}$ *there is* $d_0 > 0$ *with:*

(*a*) $\mathbf{F}$ *is Lipschitz-continuous on* $\mathcal{U}_{d_0,n}$ *with constant* $L_{\mathbf{F}} > 0$, (3.1)

(*b*) $\mathbf{G}$ *is totally differentiable with Lipschitz-continuous derivatives on* $\mathcal{U}_{d_0,n}$, (3.2)

(*c*) $\mathbf{G}_{\mathbf{z}^{(k)}}$ *(partial derivative) is invertible on* $\mathcal{U}_{d_0,n}$. (3.3)

Note, Ass. 3.1 ensures the system (2.6) to be index-1 with a well-defined solution. We prove contractivity in a smaller set $\mathcal{U}_{d,n} \subset \mathcal{U}_{d_0,n}$. — For arbitrary $\mathbf{X}, \tilde{\mathbf{X}} \in \mathcal{U}_{d_0,n}$ and k dynamic iterations on the n-th time window, we introduce the abbreviations:

$$\mathbf{Y}_n^k := \Psi_{\mathbf{y},n}^k \mathbf{X}, \quad \mathbf{Z}_n^k := \Psi_{\mathbf{z},n}^k \mathbf{X}, \quad \tilde{\mathbf{Y}}_n^k := \Psi_{\mathbf{y},n}^k \tilde{\mathbf{X}}, \quad \tilde{\mathbf{Z}}_n^k := \Psi_{\mathbf{z},n}^k \tilde{\mathbf{X}}. \tag{3.4}$$

This shorthand must not be confused with the argument of the splitting functions used in (2.10). To measure the distance after k iterations, we define the notation:

$$\begin{aligned} \Delta_{\mathbf{y}}^k(t) &:= \mathbf{Y}_n^k(t) - \tilde{\mathbf{Y}}_n^k(t), & \delta_{\mathbf{y}}^k &:= ||\Delta_{\mathbf{y}}^k|| = \max_{t_n \leq t \leq t_{n+1}} \left(\left|\Delta_{\mathbf{y}}^k(t)\right|\right), \\ \Delta_{\mathbf{z}}^k(t) &:= \mathbf{Z}_n^k(t) - \tilde{\mathbf{Z}}_n^k(t), & \delta_{\mathbf{z}}^k &:= ||\Delta_{\mathbf{z}}^k|| = \max_{t_n \leq t \leq t_{n+1}} \left(\left|\Delta_{\mathbf{z}}^k(t)\right|\right). \end{aligned} \tag{3.5}$$

These notations and the neighborhood $\mathcal{U}_{d,n}$ are visualized in Fig. 3.1.
Next we derive an estimate for the error recursion of the dynamic iteration in $\mathcal{U}_{d,n}$.

LEMMA 3.2 (Error recursion). *We consider the DAE* (2.1) *with a dynamic iteration* (2.6) *satisfying Ass. 2.1 and Ass. 3.1. We assume having reached the n-th window* $[t_n, t_{n+1}]$. *Then there are constants* $C, \tilde{c} > 1$, *such that for* $d < \min\{d_0/C,\ 1/(2\tilde{c})\}$ *and time step size* $H < H_0$ *the hypothesis*

$$\Psi_n^{k-1}\mathbf{X},\ \Psi_n^{k-1}\tilde{\mathbf{X}} \in \mathcal{U}_{d,n} \qquad (\textit{for } k \geq 1)$$

implies the recursion estimate

$$\begin{pmatrix} \delta_{\mathbf{y}}^k \\ \delta_{\mathbf{z}}^k \end{pmatrix} \leq \mathbf{K} \begin{pmatrix} \delta_{\mathbf{y}}^{k-1} \\ \delta_{\mathbf{z}}^{k-1} \end{pmatrix} + \begin{pmatrix} 1+CH \\ C \end{pmatrix} |\Delta_{\mathbf{y}}^{k-1}(t_n)| \tag{3.6}$$

with

$$\mathbf{K} := \begin{pmatrix} CH & CH \\ C & CH+\alpha_n \end{pmatrix}, \qquad \alpha_n := (1+\tilde{c}\,d)\left|\left|\mathbf{G}_{\mathbf{z}^{(k)}}^{-1}\,\mathbf{G}_{\mathbf{z}^{(k-1)}}\right|\right| + Cd. \tag{3.7}$$

Notice $\Delta_{\mathbf{y}}^{k-1}(t_n) = \Delta_{\mathbf{y}}^{0}(t_n)$ is the difference IVs for the n-th window.

Proof. The proof has two parts, corresponding to the two lines of the estimate (3.6). For the differential estimate, we write (2.6a) for both initial guesses of the dynamic iteration, $\tilde{\mathbf{X}}$ and $\mathbf{X}$. For the difference of the k-th iterate, integrated over $[t_n,\, \tau]$ (for $t_n < \tau \leq t_{n+1}$) it holds

$$|\Delta_{\mathbf{y}}^k(\tau)| \leq |\Delta_{\mathbf{y}}^{k-1}(t_n)| + L_{\mathbf{F}} \int_{t_n}^{\tau} \left\{|\Delta_{\mathbf{y}}^k| + |\Delta_{\mathbf{y}}^{k-1}| + |\Delta_{\mathbf{z}}^k| + |\Delta_{\mathbf{z}}^{k-1}|\right\} \mathrm{d}t, \tag{3.8}$$

using the solvability of the ODE (2.6a), that is guaranteed by standard arguments for a sufficiently small time window $H_n < 1/C$ (where the smallness of H_n will be concretized later on by defining C). Furthermore Lipschitz-continuity and consistency of $\mathbf{F}$ and the fact $\Delta_{\mathbf{y}}^{k-1}(t_n) = \Delta_{\mathbf{y}}^{k}(t_n)$ must be employed.

For the algebraic part in (3.8), we solve (2.6b) for $\mathbf{Z}^{(k)} = \hat{\boldsymbol{\phi}}(\mathbf{Y}^{(k)}, \mathbf{Y}^{(k-1)}, \mathbf{Z}^{(k-1)})$ (using Ass. 3.1). Lipschitz continuity of $\hat{\boldsymbol{\phi}}$ gives:

$$\begin{aligned} |\Delta_{\mathbf{z}}^k| &= |\hat{\boldsymbol{\phi}}(\mathbf{Y}^{(k)}, \mathbf{Y}^{(k-1)}, \mathbf{Z}^{(k-1)}) - \hat{\boldsymbol{\phi}}(\tilde{\mathbf{Y}}^{(k)}, \tilde{\mathbf{Y}}^{(k-1)}, \tilde{\mathbf{Z}}^{(k-1)})| \\ &\leq L_{\hat{\phi}} \left(|\Delta_{\mathbf{y}}^k| + |\Delta_{\mathbf{y}}^{k-1}| + |\Delta_{\mathbf{z}}^{k-1}|\right) \end{aligned} \tag{3.9}$$

with constant $L_{\hat{\phi}} > 0$. Inserting this result into (3.8) yields for the maximum

$$\delta_{\mathbf{y}}^k \leq |\Delta_{\mathbf{y}}^{k-1}(t_n)| + L_0\, H \left(\delta_{\mathbf{y}}^k + \delta_{\mathbf{y}}^{k-1} + \delta_{\mathbf{z}}^{k-1}\right)$$

with $L_0 := L_{\mathbf{F}}(1 + L_{\hat{\phi}})$. Thus, for $\delta_{\mathbf{y}}^k$ we find the estimate:

$$\delta_{\mathbf{y}}^k \leq \left(1 + \frac{L_0}{1 - L_0\, H}\, H\right) |\Delta_{\mathbf{y}}^{k-1}(t_n)| + \frac{L_0}{1 - L_0\, H}\, H \left(\delta_{\mathbf{y}}^{k-1} + \delta_{\mathbf{z}}^{k-1}\right). \tag{3.10}$$

For $H < H_0 := 1/(2L_0)$ we have $L_0\, H < 1/2$ and it holds

$$\delta_{\mathbf{y}}^k \leq (1 + 2L_0 H)\, |\Delta_{\mathbf{y}}^{k-1}(t_n)| + 2L_0 H \big(\delta_{\mathbf{y}}^{k-1} + \delta_{\mathbf{z}}^{k-1}\big). \tag{3.11}$$

This is the first line of estimate (3.6) for a sufficiently large constant C, see below. Using estimates (3.9) and (3.11) twice for the two particular choices: (a) $\mathbf{X} = \mathbf{x}|_{[t_n,t_{n+1}]}$ and $\tilde{\mathbf{X}}$ arbitrary, and (b) $\mathbf{X}$ arbitrary and $\tilde{\mathbf{X}} = \mathbf{x}|_{[t_n,t_{n+1}]}$, one obtains from $\mathbf{X}_n^{k-1}, \tilde{\mathbf{X}}_n^{k-1} \in \mathcal{U}_{d,n}$

$$\begin{aligned} \left|\left|\mathbf{Y}_n^k - \mathbf{y}|_{[t_n,t_{n+1}]}\right|\right|,\ \left|\left|\tilde{\mathbf{Y}}_n^k - \mathbf{y}|_{[t_n,t_{n+1}]}\right|\right| &\leq 4d, \\ \left|\left|\mathbf{Z}_n^k - \mathbf{z}|_{[t_n,t_{n+1}]}\right|\right|,\ \left|\left|\tilde{\mathbf{Z}}_n^k - \mathbf{z}|_{[t_n,t_{n+1}]}\right|\right| &\leq 6L_{\hat{\phi}}\, d. \end{aligned} \tag{3.12}$$

Thus $\mathbf{X}_n^k, \tilde{\mathbf{X}}_n^k \in \mathcal{U}_{d_0,n}$ for a sufficiently large constant $C > \max\{2L_0,\ 4,\ 6L_{\hat{\phi}}\}$.
Secondly, we establish the algebraic part of (3.6) by a homotopy; for $\theta \in [0,1]$ let

$$\mathbf{Y}^{(k),\theta}(t) := \theta\tilde{\mathbf{Y}}_n^k(t) + (1-\theta)\mathbf{Y}_n^k(t), \quad \text{and} \quad \mathbf{Z}^{(k),\theta}(t) := \theta\tilde{\mathbf{Z}}_n^k(t) + (1-\theta)\mathbf{Z}_n^k(t).$$

Inserting this in the splitting function $\mathbf{G}$, we use the abbreviation (with $\mathbf{u}$ denoting an arbitrary argument of the splitting function):

$$\mathbf{G}(\theta) := \mathbf{G}\big(\mathbf{Y}^{(k),\theta},\, \mathbf{Y}^{(k-1),\theta},\, \mathbf{Z}^{(k),\theta},\, \mathbf{Z}^{(k-1),\theta}\big) \qquad \text{and} \qquad \mathbf{G}_{\mathbf{u}}(\theta) := \frac{\partial \mathbf{G}}{\partial \mathbf{u}}(\theta).$$

Thus it holds $\mathbf{G}(0) = \mathbf{G}(1) = 0$ and therefore

$$\begin{aligned} 0 = \mathbf{G}(1) - \mathbf{G}(0) = \int_0^1 \Big(& \mathbf{G}_{\mathbf{y}^{(k)}}(\theta)\Delta_{\mathbf{y}}^k + \mathbf{G}_{\mathbf{y}^{(k-1)}}(\theta)\Delta_{\mathbf{y}}^{k-1} \\ & + \mathbf{G}_{\mathbf{z}^{(k)}}(\theta)\,\Delta_{\mathbf{z}}^k + \mathbf{G}_{\mathbf{z}^{(k-1)}}(\theta)\,\Delta_{\mathbf{z}}^{k-1}\Big)\mathrm{d}\theta. \end{aligned} \tag{3.13}$$

Employing $\frac{\partial}{\partial\theta}\mathbf{Y}^{(k),\theta} = \Delta_{\mathbf{y}}^k$ etc., Lipschitz continuity of $\mathbf{G}_{\mathbf{z}^{(k)}}$ on $\mathcal{U}_{d_0,n}$ for $Cd \le d_0$ with constant $L_{\mathbf{G}'}$ and estimate (3.12), we obtain for any time $t \in [t_n, t_{n+1}]$

$$\begin{aligned} |\mathbf{G}_{\mathbf{u}}(\theta) - \mathbf{G}_{\mathbf{u}}(0)| \;\le\; & L_{\mathbf{G}'}\Big(\big|\theta\tilde{\mathbf{Y}}_n^k(t) + (1-\theta)\mathbf{Y}_n^k(t) - \mathbf{Y}_n^k(t)\big| + \cdots + \\ & \big|\theta\tilde{\mathbf{Z}}_n^{k-1}(t) + (1-\theta)\mathbf{Z}_n^{k-1}(t) - \mathbf{Z}_n^{k-1}(t)\big|\Big) \\ =\; & L_{\mathbf{G}'}\theta\Big(|\Delta_{\mathbf{y}}^k| + |\Delta_{\mathbf{y}}^{k-1}| + |\Delta_{\mathbf{z}}^k| + |\Delta_{\mathbf{z}}^{k-1}|\Big) \\ \le\; & 12(1+L_{\hat{\phi}})L_{\mathbf{G}'}\, d. \end{aligned} \tag{3.14}$$

Ass. 3.1 guarantees that $\mathbf{G}_{\mathbf{z}^{(k)}}(0)$ is regular, thus from the estimate (3.13) we obtain by left-multiplication

$$\begin{aligned} 0 = \int_0^1 \mathbf{G}_{\mathbf{z}^{(k)}}^{-1}(0)\Big(& \mathbf{G}_{\mathbf{y}^{(k)}}(\theta)\Delta_{\mathbf{y}}^k + \mathbf{G}_{\mathbf{y}^{(k-1)}}(\theta)\Delta_{\mathbf{y}}^{k-1} + \big(\mathbf{G}_{\mathbf{z}^{(k)}}(0) + \big[\mathbf{G}_{\mathbf{z}^{(k)}}(\theta) - \mathbf{G}_{\mathbf{z}^{(k)}}(0)\big]\big)\Delta_{\mathbf{z}}^k \\ & + \big(\mathbf{G}_{\mathbf{z}^{(k-1)}}(0) + \big[\mathbf{G}_{\mathbf{z}^{(k-1)}}(\theta) - \mathbf{G}_{\mathbf{z}^{(k-1)}}(0)\big]\big)\Delta_{\mathbf{z}}^{k-1}\Big)\,\mathrm{d}\theta. \end{aligned}$$

Due to our smoothness assumptions, all operators $\mathbf{G}_{\mathbf{z}^{(k)}}^{-1}$, $\mathbf{G}_{\mathbf{z}^{(k-1)}}$, $\mathbf{G}_{\mathbf{y}^{(k)}}$, $\mathbf{G}_{\mathbf{y}^{(k-1)}}$ are uniformly bounded on $\mathcal{U}_{d_0,n}$ with constant c_g, say. Solving the last equation for $\mathbf{G}_{\mathbf{z}^{(k)}}^{-1}(0)\mathbf{G}_{\mathbf{z}^{(k)}}(0)\Delta_{\mathbf{z}}^k = \Delta_{\mathbf{z}}^k$, we obtain for the maximum norm when using (3.14):

$$\delta_{\mathbf{z}}^k \;\le \Big(||\mathbf{G}_{\mathbf{z}^{(k)}}^{-1}\,\mathbf{G}_{\mathbf{z}^{(k-1)}}|| + \frac{\tilde{c}}{2}d\Big)\,\delta_{\mathbf{z}}^{k-1} \;+\; \frac{\tilde{c}}{2}\,d\,\delta_{\mathbf{z}}^k \;+\; c_g^2\,\big(\delta_{\mathbf{y}}^k + \delta_{\mathbf{y}}^{k-1}\big),$$

where $\tilde{c} := 24(1+L_{\hat{\phi}})L_{\mathbf{G}'}c_g$ and

$$||\mathbf{G}_{\mathbf{z}^{(k)}}^{-1}\mathbf{G}_{\mathbf{z}^{(k-1)}}|| = ||\mathbf{G}_{\mathbf{z}^{(k)}}^{-1}\mathbf{G}_{\mathbf{z}^{(k-1)}}||(0) = \big|\big|\mathbf{G}_{\mathbf{z}^{(k)}}^{-1}\mathbf{G}_{\mathbf{z}^{(k-1)}}\big|\big|\big(\mathbf{Y}_n^k(t), \mathbf{Y}_n^k(t), \mathbf{Z}_n^k(t), \mathbf{Z}_n^k(t)\big).$$

Last, we use the estimate (3.11) for $\delta_{\mathbf{y}}^k$. For $H < 1/C$ and $d < \frac{1}{2\tilde{c}}$, we find

$$\begin{aligned} \delta_{\mathbf{z}}^k \;\le & 3(1+\tilde{c}d)c_g^2\Big(|\Delta_{\mathbf{y}}^{k-1}(t_n)| + \delta_{\mathbf{y}}^{k-1}\Big) \\ & + (1+\tilde{c}d)\Big(2c_g^2L_0H + ||\mathbf{G}_{\mathbf{z}^{(k)}}^{-1}\,\mathbf{G}_{\mathbf{z}^{(k-1)}}|| + \frac{\tilde{c}}{2}d\Big)\,\delta_{\mathbf{z}}^{k-1}. \end{aligned} \tag{3.15}$$

The global constant C must be large enough to deduce the self-mapping (3.12) and to deduce the error recursion claim (3.6) from estimates (3.11) and (3.15); this gives

$$C > \max\left\{2L_0,\; 4,\; 6L_{\hat{\phi}},\; 3(1+\tilde{c}d_0)c_g^2, (1+\tilde{c}d_0)c_g^2L_0,\; \frac{\tilde{c}}{2}\right\}$$

with $d > d_0$. □

The estimate for the error recursion is used to verify that the mapping defined by our dynamic iteration scheme is a fixed-point operator. In contrast to related works, the origins of the constants in the proof remain visible. This will be exploited in the

applications in Section 4f in order to achieve a better rate of convergence by enhanced modeling of the coupling interface. However, the structure of the estimate is similar to the structure of the estimates in the literature. When neglecting the special role of the initial offsets as in [3], one obtains:

REMARK 3.3. *Using* $|\Delta_{\mathbf{y}}^{k-1}(t_n)| \leq \delta_{\mathbf{y}}^{k-1}$, (3.6) *can be transformed into*

$$\begin{pmatrix} \delta_{\mathbf{y}}^{k} \\ \delta_{\mathbf{z}}^{k} \end{pmatrix} \leq \mathbf{K} \begin{pmatrix} \delta_{\mathbf{y}}^{k-1} \\ \delta_{\mathbf{z}}^{k-1} \end{pmatrix} + \begin{pmatrix} 1 \\ 0 \end{pmatrix} |\Delta_{\mathbf{y}}^{k-1}(t_n)|$$

with a possibly larger constant C *in* $\mathbf{K}$.

3.2. Convergence and stability. Based on the error recursion estimate (3.6) for general coupled DAEs (2.1) we can follow the line of [3] to investigate convergence and stability for our generalized setting. According to (3.6) the spectral radius of the iteration matrix $\rho(\mathbf{K})$ is essential for error reduction per iteration and thus for convergence. We need $\rho(\mathbf{K}) < 1$ to establish contractivity. Inspecting the eigenvalues

$$\lambda_{1,2}(\mathbf{K}) = \frac{1}{2}\Big(\alpha_n + 2\,CH \pm \sqrt{\alpha_n^2 + 4\,C^2H}\,\Big), \tag{3.16}$$

we find that $\alpha_n < 1$ is sufficient for contraction (given H small enough). This leads directly to the main contraction result:

THEOREM 3.4 (Contraction). *We consider an index-1 DAE* (2.1) *(Ass. 2.1). Let the splitting functions fulfill Ass. 3.1, let* $\mathbf{x}$ *be the analytic solution. The extrapolation operator has an accuracy of* $\mathcal{O}(H)$. *Given* $d < d_0$ *and* $H < H_0$ *small enough, then*

$$\left|\left|\mathbf{G}_{\mathbf{z}^{(k)}}^{-1}\,\mathbf{G}_{\mathbf{z}^{(k-1)}}\right|\right| < 1 \tag{3.17}$$

implies that the local error decreases with each iteration, such that the dynamic iteration Ψ *is strongly contractive.*

Notice that (3.17) implies indeed $\alpha_n < 1$ in (3.7) for d and H small enough and therefore it implies contraction.Thus, it follows from Thm. 3.4 that the local error can be made arbitrary small as $k \to \infty$.

Employing a similar estimation for the propagated error, one obtains finally:

THEOREM 3.5 (Stability). *Given a continuous extrapolation* Φ (2.4) *of accuracy order* $\mathcal{O}(H)$, *which fulfills a uniform Lipschitz condition* (L_Φ). *Let the dynamic iteration* (2.6) *be given with consistent splitting functions* $\mathbf{F}$, $\mathbf{G}$, *which satisfy the Ass. 3.1 on* $[t_n, t_{n+1}]$. *Furthermore let the contractivity constants be bounded*

$$\alpha_n \leq \bar{\alpha} < 1 \qquad \text{and} \qquad L_\Phi \alpha_n^{k_n} \leq \bar{\alpha}$$

and the numerical approximations (before the n-th time window) stay in the neighborhood of the exact solution. Then the global error on the time window $[t_n, t_{n+1}]$ *is smaller than d for all window size* $0 < H < H_0$ *small enough.*

3.3. Rate of convergence. We have seen that $\rho(\mathbf{K})$ governs (the speed of) convergence. Now as rate of convergence of the dynamic iteration (2.6), we inspect the asymptotics of the eigenvalues of $\mathbf{K}$ (3.7) as $H \to 0$. This gives rise to the following discussion of $\rho(\mathbf{K})$ for different coupling structures what then leads to a corollary for Thm. 3.4. Finally, we are able to identify former results from literature as special cases of our generalized approach.

REMARK 3.6 (Convergence rate of fixed point iteration).

(i) A Taylor expansion of the square root in $\lambda(\mathbf{K})$ (3.16) *yields*

$$\sqrt{\alpha_n^2 + 4\,C^2H} = \alpha_n\,(1 + 2\,C^2H/\alpha_n^2) + \mathcal{O}(H^2).$$

Thus, if $\alpha_n \neq 0$ *and* $4\,C^2H < \alpha_n^2$, *then the rate is* $\alpha_n + \mathcal{O}(H)$.

(ii) The convergence of the distributed DAE-time integration requires also the stability of the coupling of algebraic to algebraic components (3.17).

(iii) The computational sequence of the subsystems is reflected in the splitting functions; thus (3.17) *may change for different sequences, e.g. when using a Gauss-Seidel scheme (see Section 6.2 for a computational example).*

If possible, the modeling of distributed time integration of coupled DAEs should be performed such that contraction is directly ensured – as for example in the following special cases. Here contraction is guaranteed by inspecting the structure of the coupling (cf. [5]). The results are obtained by following the lines of the proof of Lem. 3.2 but exploiting the special cases.

COROLLARY 3.7 (Simple coupling). *We assume the hypothesis of Lem. 3.2.*

i) Given a splitting, where no algebraic constraint depends on an old algebraic iterate, that is,

$$\mathbf{G}_{\mathbf{z}^{(k-1)}} = 0, \tag{3.18}$$

then $\alpha_n = 0$ and contraction follows with rate $\mathcal{O}(\sqrt{H})$.

ii) Given a splitting, where no algebraic constraint depends on old iterates, i.e.,

$$\mathbf{G}_{\mathbf{z}^{(k-1)}} = 0 \quad \textit{and} \quad \mathbf{G}_{\mathbf{y}^{(k-1)}} = 0, \tag{3.19}$$

then contraction follows with rate $\mathcal{O}(H)$.

REMARK 3.8 (Fractional step). *Cor. 3.7i) includes the special case of a Gauss-Seidel-type iteration scheme for a semi-explicit DAE (index-1), where one subsystem is the ODE and the other subsystem is the algebraic equation, i.e.,*

$$\mathbf{F} := \mathbf{f}(\mathbf{y}^{(k)}, \mathbf{z}^{(k-1)}) \quad \textit{and} \quad \mathbf{G} := \mathbf{g}(\mathbf{y}^{(k)}, \mathbf{z}^{(k)}). \tag{3.20}$$

For this so called 'fractional step method' applied to index-1 DAEs, the convergence rate $\mathcal{O}(H)$ has been proven independently, [28].

4. Applications in electric circuit simulation. In circuit simulation, e.g. [10], electromagnetic devices and semiconductor devices are modeled as a network of idealized basic elements (resistors, inductors, capacitors and sources). The network ansatz yields a system of DAEs, such that the entire circuit can be simulated using common circuit simulation tools. However, many devices cannot be given sufficiently accurate in terms of idealized lumped elements. This requires the hierarchical coupling of PDE device models to the network. Space-discretization turns this into a DAE-DAE coupled problem.

The common monolithic simulation is often cumbersome or sometimes even impossible due to incompatible simulation tools. For example, a circuit simulator and a device simulator may not have interfaces to interchange all necessary data during transient simulations (e.g. the Jacobians must be interchanged). On the other hand, the injection of lumped parameters, i.e., currents, into the circuit simulator is not a problem. This will be exploited by the co-simulation scheme given below.

4.1. Electric circuit model. Circuit simulators are commonly based on the flux/charge oriented modified nodal analysis (MNA), see e.g. [14]:

$$\mathbf{A}_{\mathrm{C}}\frac{\mathrm{d}}{\mathrm{d}t}\mathbf{q} + \mathbf{A}_{\mathrm{R}}\mathbf{g}_{\mathrm{R}}(\mathbf{A}_{\mathrm{R}}^{\top}\mathbf{u}, t) + \mathbf{A}_{\mathrm{L}}\mathbf{i}_{\mathrm{L}} + \mathbf{A}_{\mathrm{V}}\mathbf{i}_{\mathrm{V}} + \mathbf{A}_{\mathrm{I}}\mathbf{i}(t) + \mathbf{A}_{\mathrm{D}}\mathbf{i}_{\mathrm{D}} = \mathbf{0}, \tag{4.1a}$$

$$\frac{\mathrm{d}}{\mathrm{d}t}\mathbf{\Phi} - \mathbf{A}_{\mathrm{L}}^{\top}\mathbf{u} = \mathbf{0}, \qquad \mathbf{A}_{\mathrm{V}}^{\top}\mathbf{u} - \mathbf{v}(t) = \mathbf{0}, \tag{4.1b}$$

$$\mathbf{q} - \mathbf{q}_{\mathrm{C}}(\mathbf{A}_{\mathrm{C}}^{\top}\mathbf{u}, t) = \mathbf{0}, \qquad \mathbf{\Phi} - \mathbf{\Phi}_{\mathrm{L}}(\mathbf{i}_{\mathrm{L}}, t) = \mathbf{0}, \tag{4.1c}$$

where $\mathbf{q}_{\mathrm{C}}(\mathbf{v},t)$, $\mathbf{g}_{\mathrm{R}}(\mathbf{v},t)$, $\mathbf{\Phi}_{\mathrm{L}}(\mathbf{i},t)$, $\mathbf{v}_{\mathrm{S}}(t)$ and $\mathbf{i}_{\mathrm{S}}(t)$ denote the element contributions as charges, currents of resistors, fluxes, voltage and current sources, respectively. The matrices $\mathbf{A}_\star$ denote network incidences and finally $\mathbf{i}_{\mathrm{D}}$ is the injected current from the semiconductor or field device (simulator) as discussed below. The unknowns of the circuit model equations are charges $\mathbf{q}(t)$, fluxes $\mathbf{\Phi}(t)$, currents $\mathbf{i}_{\mathrm{L}}(t)$, $\mathbf{i}_{\mathrm{V}}(t)$ through inductors and voltage sources as well as all node potentials $\mathbf{u}(t)$ except ground.

In the following, we assume the standard conditions, such that the circuit equations (4.1) are of index-1 for a given function $\mathbf{i}_{\mathrm{D}}(t)$: namely, locally positive definite element contributions and there exists neither a CV-loop nor an LI-cutset [13].

4.2. Coupling settings. Next, we apply the theoretical results from the sections above to the case of a circuit coupled to two different devices of very different scale: in Sections 5–7 the semiconductor-circuit coupling, where we use a 1D PDE model of a *pn*-diode and in Sections 8–10 the field-circuit coupling, where we employ a 2D model of a transformer. In both cases, different coupling techniques and interfaces are discussed: (A) source coupling, and (B) coupling using extracted, lumped parameters. The source coupling approach represents a black-box coupling where the circuit does not see the physics of the device. The lumped parameter approach on the other hand includes further physical effects. It fits into the framework of [12] where compact models are used as predictor in the coupled simulation. Moreover, it is related to the DIRM approach: dynamic iteration using reduced order models, [22].

Furthermore, we will show that the sequence of solving the subsystems can be crucial for convergence of the iteration. Thus we discuss: (i) device-first, (ii) circuit-first. Finally, we investigate the convergence rate of the fixed point iteration in terms of the time window size in the mentioned cases.

5. Semiconductor-circuit coupling. First we state the drift-diffusion model (spatially discretized). Then we discuss the two types of circuit coupling.

5.1. Semiconductor model. The *pn*-diode in our example is described by the domain $\Omega \subset \mathbb{R}^d$ for $d = 1, 2, 3$ with $\partial\Omega = \Gamma = \Gamma_D \cup \Gamma_N$. Its physical behavior is modeled by the drift-diffusion (DD) model, which consists of conservation laws for the electron and hole densities coupled to the Poisson equation for the electric potential [26]. To ensure non-negativity of the carrier densities, the DD-equations are discretized using exponentially fitted mixed finite elements as described in [19, 8]. Thus the discretized DD-equations read

$$\mathbf{A}_{\mathrm{n}}(\mathbf{V})\frac{\mathrm{d}}{\mathrm{d}t}\mathbf{n} + \mathbf{B}_{\mathrm{n}}(\mathbf{p},\mathbf{V})\mathbf{n} = \mathbf{f}_{\mathrm{n}}(\mathbf{p},\mathbf{V}), \quad \mathbf{A}_{\mathrm{p}}(\mathbf{V})\frac{\mathrm{d}}{\mathrm{d}t}\mathbf{p} + \mathbf{B}_{\mathrm{p}}(\mathbf{n},\mathbf{V})\mathbf{p} = \mathbf{f}_{\mathrm{p}}(\mathbf{n},\mathbf{V}), \quad (5.1a)$$

$$\mathbf{L}\mathbf{V} = \mathbf{n} - \mathbf{p} - \mathbf{C} + \mathbf{f}_{\mathrm{V}}(\mathbf{v}_{\mathrm{D}}), \quad (5.1b)$$

$$\mathbf{i}_{\mathrm{D}} = \mathrm{j}_{\mathrm{D}}(\mathbf{n},\mathbf{p},\mathbf{V}), \quad (5.1c)$$

with regular matrices $\mathbf{A}_{\mathrm{n}}, \mathbf{A}_{\mathrm{p}}, \mathbf{B}_{\mathrm{n}}, \mathbf{B}_{\mathrm{p}}, \mathbf{L}$ (cf. [8, 2]). Here $\mathbf{n}, \mathbf{p}, \mathbf{C}$ and $\mathbf{V}$ denote the discrete approximations of the electron and hole density, the doping profile and the potential. The applied voltage drop is given by $\mathbf{v}_{\mathrm{D}}$. The total current leaving the device $\mathbf{i}_{\mathrm{D}}$ takes into account the particle current as well as the displacement current. The employed boundary conditions for the system are incorporated in the functions $\mathbf{f}_{\mathrm{n}}, \mathbf{f}_{\mathrm{p}}$ and $\mathbf{f}_{\mathrm{V}}$, for details we refer to [2]. We note that standard finite element or finite difference discretization would allow for a similar representation.

Alternatively the displacement current can be expressed in terms of a capacitance C_{D} and the time derivative of the applied voltage drop [1]. Instead of (5.1c) the total

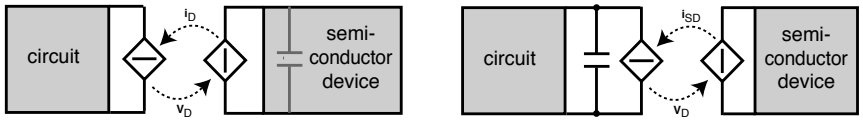

(a) Source coupling. (b) Coupling with capacitance.

Figure 5.1: Displacement current modeled inside the PDE device (A) and by capacitance extraction in circuit (B), see [2].

current can be written as

$$\mathbf{i}_{\mathrm{D}} = C_{\mathrm{D}} \frac{\mathrm{d}}{\mathrm{d}t} \mathbf{v}_{\mathrm{D}} - \mathbf{i}_{\mathrm{SD}} \quad \text{with} \quad \mathbf{i}_{\mathrm{SD}} := j_{\mathrm{SD}}(\mathbf{n}, \mathbf{p}, \mathbf{V}). \tag{5.1d}$$

In case of a 1D model for a cubic diode with length l and cross-section A, it holds: $C_{\mathrm{D}} = \epsilon_s \cdot A/l$, where ϵ_s denotes the material's permittivity.

5.2. Coupling types. The structure of the equations allows for two different representations: (A) coupling by plain sources (*source coupling*), in which the displacement current is considered as part of the distributed device model, i.e., $\mathbf{i}_{\mathrm{D}}$ is defined by (5.1c), or, (B) coupling, where the displacement current is described in terms of circuit variables, i.e., (5.1d) is treated as an additional circuit equation (*coupling with capacitance*), see Fig. 5.1. In both settings the voltage drop $\mathbf{v}_{\mathrm{D}}$ in the circuit describes the boundary condition for the electric potential $\mathbf{V}$ in the device model. In the case of a monolithic coupling, those two representations are equivalent, but in the case of a weak coupling by a dynamic iteration scheme, they exhibit different behavior. Since the additional capacity C_D in the circuit model (in setting (B)) can be considered as simple compact model for the capacitive behavior of the diode, the *coupling with capacitances* reflects compact model design.

A. Source coupling. For given $\mathbf{v}_{\mathrm{D}}$ the spatial discretization of the DD-equations (5.1) yields an index-1 DAE [8]. Moreover, we assume the coupled system to be of index-1 [25], i.e., no additional CV-loop is introduced by the coupling. Then the system can be written in semi-explicit form: (d for device and c for circuit)

$$\begin{aligned} \dot{\mathbf{y}}_d &= \mathbf{f}_d(\mathbf{y}_d, \mathbf{z}_d), & \dot{\mathbf{y}}_c &= \mathbf{f}_c(\mathbf{y}_c, \mathbf{z}_c, \mathbf{z}_d), \\ \mathbf{0} &= \mathbf{g}_d(\mathbf{y}_d, \mathbf{z}_d, \mathbf{z}_c), & \mathbf{0} &= \mathbf{g}_c(\mathbf{y}_c, \mathbf{z}_c, \mathbf{z}_d), \end{aligned} \tag{5.2}$$

with regular $\partial \mathbf{g}_d / \partial \mathbf{z}_d$ and $\partial \mathbf{g}_c / \partial \mathbf{z}_c$. The differential variables of the diode and circuit are $\mathbf{y}_d := (\mathbf{n}, \mathbf{p})$ and $\mathbf{y}_c := (\mathbf{q}, \mathbf{\Phi})$, whereas the corresponding algebraic unknowns are $\mathbf{z}_d = (\mathbf{V}, \mathbf{i}_{\mathrm{D}})$ and $\mathbf{z}_c := (\mathbf{u}, \mathbf{i}_{\mathrm{L}}, \mathbf{i}_{\mathrm{V}})$. Here the device current $\mathbf{i}_{\mathrm{D}}$ is defined by (5.1c).

In fact, the spatial discretization by the positivity-preserving mixed finite element scheme might turn some components of $\mathbf{n}, \mathbf{p}$ into algebraic variables [8]. However, this would not affect our iteration scheme as long as the index-1 assumptions hold.

In this setting all node potentials $\mathbf{u}$ and thus $\mathbf{v}_{\mathrm{D}} = \mathbf{A}_{\mathrm{D}}^{\top} \mathbf{u}$ are algebraic variables of the circuit. Thus the algebraic equations of the device $\mathbf{0} = \mathbf{g}_d$ only depend on the algebraic variable $\mathbf{z}_c$ of the circuit. The diode current is also algebraic, but, depending on the circuit's topology, it may appear in the differential $\mathbf{f}_c$ as well as in the algebraic equation $\mathbf{g}_c$ of system (5.2).

B. Coupling with capacitance. Now, we use the definition of $\mathbf{i}_{\mathrm{D}}$ from (5.1d) in the current balance equation (4.1a). This leads to a slightly different system:

$$\begin{aligned} \dot{\mathbf{y}}_d &= \mathbf{f}_d(\mathbf{y}_d, \mathbf{z}_d), & \dot{\mathbf{y}}_c &= \mathbf{f}_c(\mathbf{y}_c, \mathbf{z}_c, \mathbf{z}_d), \\ \mathbf{0} &= \mathbf{g}_d(\mathbf{y}_d, \mathbf{z}_d, \mathbf{y}_c), & \mathbf{0} &= \mathbf{g}_c(\mathbf{y}_c, \mathbf{z}_c), \end{aligned} \tag{5.3}$$

with differential unknowns $\mathbf{y}_d := (\mathbf{n}, \mathbf{p})$ and $\mathbf{y}_c := (\mathbf{q}, \mathbf{\Phi}, \mathbf{P}_D \mathbf{u})$ and algebraic unknowns $\mathbf{z}_d = (\mathbf{V}, \mathbf{i}_{\mathrm{SD}})$ and $\mathbf{z}_c := (\mathbf{Q}_D \mathbf{u}, \mathbf{i}_{\mathrm{L}}, \mathbf{i}_{\mathrm{V}})$. Here $\mathbf{Q}_D$ denotes a projector onto

the kernel of $\mathbf{A}_{\mathrm{D}}^{\top}$ and $\mathbf{P}_D$ its complement, as they typically appear in circuit index analysis, [13]. In this formulation the node potentials are split, since the capacitance C_D is not written in charge oriented form. Due to the linearity of C_D the advantage of the charge/flux oriented MNA, i.e., charge conservation, is still respected.

As a result of the capacitive path between the coupling nodes, $\mathbf{v}_{\mathrm{D}}$ is part of the differential variables $\mathbf{y}_c$ and the algebraic equations of the device subsystem only depend on differential circuit variables. In turn, the device current $\mathbf{i}_{\mathrm{SD}}$ — an algebraic device variable — enters differential equations $\mathbf{f}_c$ of the circuit subsystem, only.

6. Dynamic iteration for the semiconductor-circuit system. Based on the theory above, we discuss the convergence properties of the dynamic iteration in this application. First we investigate the coupling types (A) and (B). Then the influence of the subsystem's computational sequence is studied (for type (B) only).

6.1. Coupling types in the dynamic iteration. We distinguish two types:

A. Source coupling. Here the two subsystems in (5.2) are coupled via algebraic variables $\mathbf{z}_\star$ in the algebraic equations $\mathbf{g}_\star$. Independent of the sequence of the subsystems in a dynamic iteration scheme, i.e., circuit-first or device-first, we always observe a dependence of the algebraic equation (iteration k) on old algebraic variables $(k-1)$. This holds true for Jacobi-Iteration as well as a Gauß-Seidel approach. For the device-first approach, the Gauss-Seidel scheme reads

$$\mathbf{F} := \begin{bmatrix} \mathbf{f}_d(\mathbf{y}_d^{(k)}, \mathbf{z}_d^{(k)}) \\ \mathbf{f}_c(\mathbf{y}_c^{(k)}, \mathbf{z}_c^{(k)}, \mathbf{z}_d^{(k)}) \end{bmatrix} \qquad \text{and} \qquad \mathbf{G} := \begin{bmatrix} \mathbf{g}_d(\mathbf{y}_d^{(k)}, \mathbf{z}_d^{(k)}, \mathbf{z}_c^{(k-1)}) \\ \mathbf{g}_c(\mathbf{y}_c^{(k)}, \mathbf{z}_c^{(k)}, \mathbf{z}_d^{(k)}) \end{bmatrix}, \tag{6.1}$$

where the superscript (k) denotes the iteration number. Since $\mathbf{G}$ depends on an old algebraic iterate the contraction factor α does not vanish, see (3.7). Thus convergence cannot be guaranteed by the structural analysis. The parameters of device and circuit will have a serious influence. This is discussed for an numerical example in Section 7.

B. Coupling with capacitance. Here, in system (5.3), the capacitance C_D is parallel to the device. The coupling of the two subsystems in the algebraic equations only happens in terms of differential variables, i.e., $\mathbf{g}_d$ depends on $\mathbf{y}_c$. According to Corollary 3.7 and Remark 3.6, convergence of the dynamic iteration is guaranteed for time windows size H small enough. Independent of the sequence of the subsystems, we will observe a dynamic iteration with convergence rate $\mathcal{O}(\sqrt{H})$ for $H \to 0$, for a Jacobi-Iteration approach.

According to Corollary 3.7, for the Gauß-Seidel approach we expect convergence rate $\mathcal{O}(H)$ if we start the iteration scheme by computing the circuit-subsystem first, since in this case the algebraic functions do not depend on old differential variables. If we exchange the sequence of the subsystems, i.e., start the iteration by computing the device subsystem first, and use the Gauß-Seidel approach, according to Remark 3.6 we only can guarantee convergence rate $\mathcal{O}(\sqrt{H})$.

However, the structure considered in the theory above is rather general and our two subsystems observe less dependencies than the general case. Thus, we shortly address the two cases of Gauß-Seidel iteration for the system (5.3), i.e., circuit-first and device-first with the technique used above, in order to get a more detailed statement about the convergence rate of the fixed point iteration (3.7) in semiconductor-circuit coupled applications.

6.2. Analysis of the sequence of the subsystems. In this section, we only address case B, i.e., system (5.3), and assume that its two subsystems are of index 1. Then the functions $\mathbf{g}_c, \mathbf{g}_d$ are uniquely solvable with respect to $\mathbf{z}_c$ and $\mathbf{z}_d$, respectively.

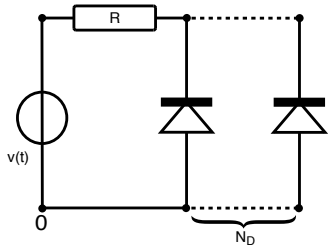

(a) Example circuit

Parameter	Physical meaning
$q = 1.6 \cdot 10^{-19}\,\mathrm{As}$	elementary charge
$\epsilon_s = 10^{-10}\,\mathrm{As/Vm}$	permittivity constant
$U_T = 0.026\,\mathrm{V}$	thermal voltage at $T_L = 300K$
$\mu_n/\mu_p = 0.15/0.045\,\mathrm{m^2/Vs}$	low-field carrier mobilities
$C_0 = 10^{23}\,\mathrm{m}^{-3}$	maximum doping concentration
$l = 10^{-7}\,\mathrm{m}$	length
$A = 10^{-14}\,\mathrm{m}^2$	cross-section

(b) Physical parameters for a silicon *pn*-junction diode.

Figure 6.1: Circuit and device parameters.

We furthermore assume the functions $\mathbf{f}_c$ and $\mathbf{f}_d$ to be Lipschitz-continuous in $\mathcal{U}_{d_0,n}$ (see also Ass. 3.1) with respect to all its components. Additionally, the implicit functions Φ_c and Φ_d determining $\mathbf{z}_c$ and $\mathbf{z}_d$ shall be Lipschitz-continuous.

DEFINITION 6.1 (Lipschitz constants). *We define the following abbreviations:*
L: Maximum of the Lipschitz constants of $\mathbf{f}_\star$ and $\Phi_\star$ w.r.t. $\mathbf{y}_\star$ and $\mathbf{z}_\star$ for $\star \in \{d, c\}$.
L_c: Maximum of L and the Lipschitz constant of $\mathbf{f}_c$ w.r.t. $\mathbf{z}_d$.
L_d: Maximum of L and the Lipschitz constant of Φ_d w.r.t. $\mathbf{y}_c$.

We note that the Lipschitz constants L_d and L_c can be regarded as the measure for the strength of the coupling between the two subsystems with respect to differential and algebraic variables, respectively.

LEMMA 6.2 (Circuit-Device error recursions). *(i) For the Gauss-Seidel scheme applied to* (5.3) *with device-first, the error recursion according to* (3.6) *reads*

$$\begin{pmatrix} \delta_{\mathbf{y}}^k \\ \delta_{\mathbf{z}}^k \end{pmatrix} \leq \underbrace{\begin{pmatrix} C_d H & 0 \\ C & 0 \end{pmatrix}}_{=:\mathbf{K_D}} \begin{pmatrix} \delta_{\mathbf{y}}^{k-1} \\ \delta_{\mathbf{z}}^{k-1} \end{pmatrix} + \begin{pmatrix} 1 + CH \\ C \end{pmatrix} |\Delta_{\mathbf{y}}^{k-1}(t_n)|. \tag{6.2}$$

(ii) The circuit-first Gauss-Seidel scheme applied to (5.3) *yields the error recursion:*

$$\begin{pmatrix} \delta_{\mathbf{y}}^k \\ \delta_{\mathbf{z}}^k \end{pmatrix} \leq \underbrace{\begin{pmatrix} 0 & CH \\ 0 & C_c H \end{pmatrix}}_{=:\mathbf{K_C}} \begin{pmatrix} \delta_{\mathbf{y}}^{k-1} \\ \delta_{\mathbf{z}}^{k-1} \end{pmatrix} + \begin{pmatrix} 1 + CH \\ C \end{pmatrix} |\Delta_{\mathbf{y}}^{k-1}(t_n)|. \tag{6.3}$$

Thereby it holds

$$C_d = \frac{L_c L_d}{1 - L(1 + L_c)H_0}, \qquad C_c = \frac{L_c L_d}{1 - L(1 + L_d)H_0}, \tag{6.4}$$

with the maximum time window size H_0 and a suitable constant $C > 0$.

Proof. This lemma is proven analogously to Lemma 3.2. The only difference is, that we distinguish between the Lipschitz constants, here. □

THEOREM 6.3. *For the coupled semiconductor-circuit system with capacitance coupling* (5.3) *using a Gauss-Seidel dynamic iteration, the fixed point iteration is convergent with convergence rate $\mathcal{O}(H)$ for $H \to 0$. This holds independently of the computational sequence and on each time window. The leading order coefficients can be estimated by C_d and C_c, given in* (6.4).

Proof. Convergence follows immediately from Corollary 3.7. The spectral radius of the iteration matrix $\mathbf{K_D}$ is given by $\rho(\mathbf{K_D}) = C_d H$. Thus we expect the convergence rate $C_d H$ for the device-first approach. Analogously the spectral radius of the iteration matrix $\mathbf{K_C}$ in (6.3) is given by $\rho(\mathbf{K_C}) = C_c H$ and thus we expect the convergence rate $C_c H$ for the circuit-first approach. □

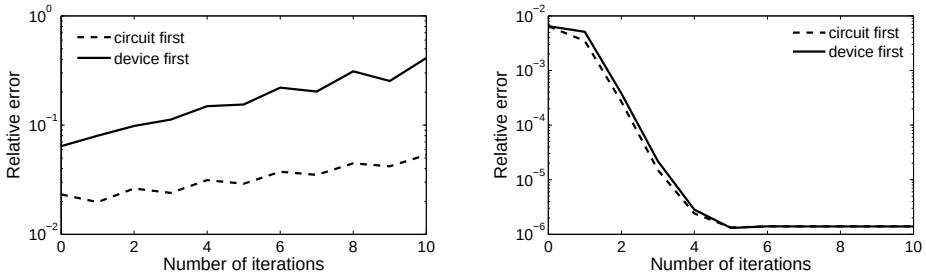

(a) Source coupling. (b) Coupling with capacitance.

Figure 7.1: Relative error of network components between 2.2–$2.3 \cdot 10^{-12}$s.

REMARK 6.4. *Due to the special structure of our coupled semiconductor-circuit problem, we obtain convergence rate $\mathcal{O}(H)$ for the device-first approach, even if we observe a dependency of the algebraic constraints on old differential variables.*

The speed of convergence of the dynamic iteration scheme depends on the leading order coefficients C_c and C_d. Thus it strongly depends on the constants L_c and L_d, which reflect the strength of the coupling via differential and algebraic variables and equations, respectively. The symmetry of C_c and C_d with respect to L_c and L_d can be observed in (6.4). Obviously, the device-first approach has a slower convergence for large L_c than the other case. This reflects a strong dependence of the circuit equations on the device model. Vice versa, we get an increasing constant C_c for the circuit-first approach, for large L_d. Below, this behavior will be verified by simulations.

7. Numerical results. We visualize the above results by the simulation of a series connection of a voltage source, a resistor and a block of several (1D-modeled) silicon *pn*-diodes connected in parallel, see Fig. 6.1a. The circuit parameters are: resistance $R = 1\Omega$, the voltage source $v(t) = \sin(\omega t)$V with $\omega = 2\pi 10^{11}$ Hz. Each diode consists of a 50 nm n-region doped with C_0 and a 50 nm p-region doped with $-C_0$. Further parameters of the diode are given in Fig. 6.1b.

First we assume that the diode-block consists of 1500 identical diodes in parallel. Due to the parallel connection, accurate results are obtained by calculating one diode only and multiplying the output current by the number of devices.

7.1. Convergence study of coupling types. In the following simulations we applied a backward Euler with constant time step size of $\Delta t = 0.1 \cdot 10^{-12}$s and simulate our circuit until $T = 10 \cdot 10^{-12}$s. The choice of the Euler scheme is merely to due the fact that we want to verify our analytic results unbiased (from other effects). On each time window $H = \Delta t$ (i.e., each window is solved using exactly one step), we accomplish 10 iterations and compare the network variables computed with our dynamic iteration scheme below, to a monolithic reference solution. The reference solution is made to verify the convergence of the dynamic iteration scheme to the solution of the monolithic systems. Therefore it is computed with same step size but strongly coupled. For details of the algorithm we refer to [2].

A. Source coupling. The dynamic iteration for this coupling approach applied to the example circuit (Fig. 6.1) does not converge. In Fig. 7.1a, we depict the relative error of the network components, i.e., the deviation from the reference solution, against the number of iterations in the time interval 2.2–$2.3 \cdot 10^{-12}$s. We choose this interval, since there the simulation breaks down. For both sequences — device or circuit first — the iteration scheme clearly diverges. The different starting values for

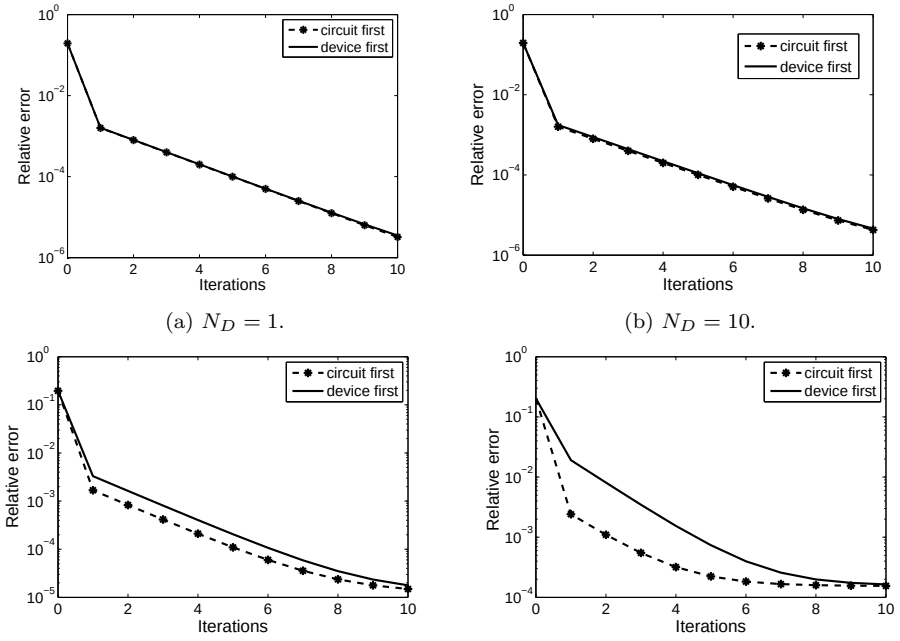

(a) $N_D = 1$. (b) $N_D = 10$.

(c) $N_D = 100$. (d) $N_D = 1000$.

Figure 7.2: Relative error between 0.4–$0.5 \cdot 10^{-12}$s for different numbers of diodes. From upper left to lower right : $N_D = 1, 10, 100, 1000$.

the two different sequences (Fig. 7.1a) are due to bad convergence in the previous time windows and are the result of error propagation. We note that the amplification of the diode current by the factor of 1500 (due to the 1500 devices in parallel) causes the crucial parameter α in (3.7) to be greater than one, what results in divergence.

B. Coupling with capacitance. Here, we extract the capacitive behavior of each diode as a parallel capacitance $C_{\mathrm{D}} = 10^{-17}$ F. This results in an overall capacitance of $1.5 \cdot 10^{-14}$ F for the circuit subsystem. In turn, we compute the diode current $\mathbf{i}_{\mathrm{SD}}$ without displacement contribution. In contrast to the source coupling approach, we observe a convergent algorithm. In Fig. 7.1b we depict the relative error (i.e., the relative deviation from the monolithic reference solution) of the network components against the number of iterations in the interval 2.2–$2.3 \cdot 10^{-12}$s, where the source coupling algorithm broke down. Clearly, we get convergence with the capacitance in parallel. Moreover, we observed significantly better convergence on the previous time windows.

7.2. Sequence study. We investigate the influence of the sequence of the subsystems onto the speed of convergence of the dynamic iteration scheme. Therefore, we simulate the circuit given above for different numbers of parallel diodes, namely $N_D = 10$, 100 and 1000 devices. The number of devices is reflected by the Lipschitz-constant L_c, i.e., for increasing N_D the Lipschitz-constant L_c is increasing.

In Fig. 7.2 we depict the convergence of the dynamic iteration scheme on one time window (we have chosen time window number 5) against the reference solution computed for respective number of diodes. Again, we used a time step size $\Delta t = 0.1 \cdot 10^{-12}$s. For the monolithic reference solution we applied the same step size. Fig 7.2 shows that for few diodes the speed of convergence is almost the same for both approaches. However, for more diodes the speed of convergence of the circuit-

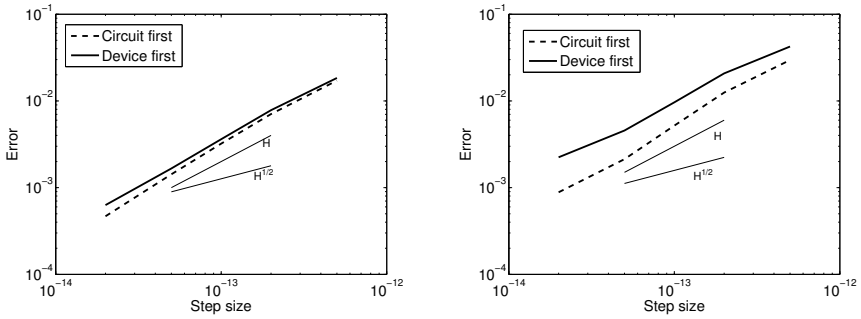

(a) $N_D = 100$. (b) $N_D = 1000$.

Figure 7.3: Splitting error for different values of L_c after $2 \cdot 10^{-12}$s for different time window sizes and for the circuit first6and device first approach with one iteration per time window.

first approach becomes faster. For 100 diodes we get the same accuracy with one iteration less for the circuit-first approach. For $N_D = 1000$ diodes we seem to save even two iterations by using the circuit-first approach. Those results reflect the leading order coefficients C_d and C_c given in (6.4).

We note that for increasing value of L_d we expect the device-first approach to be superior. This shows the importance of a proper estimation of the strength of the coupling, i.e., a proper estimation of the Lipschitz constants L_c, L_d, since by the value of those constant we can determine the optimal sequence for solving the subsystems.

Finally, we investigate the rate of convergence for our coupled simulation. To this end, we simulate the above introduced system for $2 \cdot 10^{-12}$s with capacitance coupling using either circuit-first or device-first approach. We only apply one Gauß-Seidel iteration per time window (i.e. $k_n = 1$). For time integration we use the first order implicit Euler method. According to the theory, we expect convergence rate $\mathcal{O}(H)$ (for window size $H \to 0$) already after one iteration of the dynamic iteration scheme on one window, for both approaches.

Fig. 7.3 shows that both approaches yield a convergence rate in the order of the time window size H. Additionally, we see that for the larger Lipschitz-constants L_c the circuit-first approach performs slightly better, as expected from Theorem 6.3.

8. Magnetostatic coupling. We come to a second application where we consider the simulation of magnetic fields. Especially to optimize and analyze geometry, nonlinearity etc., the coupling of electric networks with distributed models of electrical machines, e.g. transformers, is important, [27].

For low-frequencies the electric displacement currents and the resistive eddy currents can be neglected in comparison to the currents induced by the magnetic field. This yields the *magnetostatic* approximation of Maxwell's equations. We will use dynamic iteration for coupled magnetostatic-devices and electric circuits. Thereby we fit a lumped compact model (inductor) for the behavior of the magnetostatic PDE model of a transformer. This approach works analogously for other devices and applications (as we have seen in the semiconductor-circuit coupling) and it is shown to be very efficient when multirate behavior is exploited, [24]. After stating the model, we examine its convergence properties, here.

8.1. Field device model. The transformer in our example circuit, Fig. 8.1a, is described on a bounded 2D-domain $\Omega \subset \mathbb{R}^2$, Fig. 8.1b. Its physical behavior is described by a magnetostatic model, which is discretized in space using Whitney

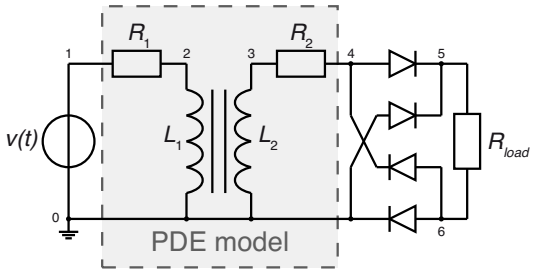

(a) Rectifier circuit, with four lumped diode models, winding and load resistance.

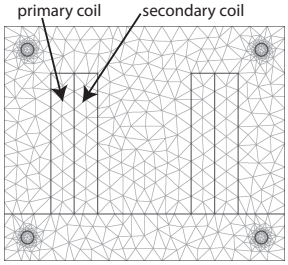

(b) Transformer PDE model, discretized by FEMM, [20].

Figure 8.1: Nonlinear transformer embedded in nonlinear rectifier circuit.

elements, see [7]. Then the discretized device problem for the line-integrated magnetic vector potentials $\mathbf{a}$ reads

$$\mathbf{K}_\nu(\mathbf{a})\mathbf{a} = \mathbf{X}_\mathrm{D}\mathbf{i}_\mathrm{D}, \tag{8.1}$$

which is equipped with circuit coupling equations, e.g. [23]

$$\frac{\mathrm{d}}{\mathrm{d}t}\mathbf{\Phi}_\mathrm{D} + \mathbf{R}_\mathrm{D}\mathbf{i}_\mathrm{D} = \mathbf{v}_\mathrm{D} \qquad \text{with} \qquad \mathbf{\Phi}_\mathrm{D} := \mathbf{X}_\mathrm{D}^\top\mathbf{a}. \tag{8.2}$$

Here $\mathbf{R}_\mathrm{D}$ denotes the device's DC resistances, $\mathbf{i}_\mathrm{D} = \mathbf{A}_\mathrm{D}\mathbf{i}$ and $\mathbf{v}_\mathrm{D} = \mathbf{A}_\mathrm{D}^\top\mathbf{v}$ are the currents and voltage drops of the coil windings, and $\mathbf{\Phi}_\mathrm{D}$ represents the magnetic flux. Each column of the matrix $\mathbf{X}_\mathrm{D}$ is a spatial discretization of a winding function, such that $\mathbf{X}_\mathrm{D}\mathbf{i}$ describes the spatial distribution of the applied currents $\mathbf{i}$. The curl-curl matrix $\mathbf{K}_\nu := \mathbf{C}^\top\mathbf{M}_\nu\mathbf{C}$ depends nonlinearly on the magnitude of the discrete flux density via the reluctivity to model saturation: $\mathbf{M}_\nu = \mathbf{M}_\nu(|\mathbf{C}\mathbf{a}|)$ with the discrete curl operator $\mathbf{C}$. Finally, the unknowns of the field system are $(\mathbf{a}, \mathbf{\Phi}_\mathrm{D}, \mathbf{i}_\mathrm{D})$. Note that in simulations $\mathbf{\Phi}_\mathrm{D}$ is not explicitly computed similar to flux-charged oriented MNA.

For a known solution $\mathbf{a}^\star$ of (8.1), we can invert $\mathbf{K}_\nu(\mathbf{a}^\star)$, insert the result into the definition of $\mathbf{\Phi}_\mathrm{D}$, (8.2), and finally replace $\mathbf{\Phi}_\mathrm{D}$ in (8.2):

$$\frac{\mathrm{d}}{\mathrm{d}t}\big(\mathbf{L}_\mathrm{D}\mathbf{i}_\mathrm{D}\big) + \mathbf{R}_\mathrm{D}\mathbf{i}_\mathrm{D} = \mathbf{v}_\mathrm{D} \qquad \text{with} \qquad \mathbf{L}_\mathrm{D} := \mathbf{X}_\mathrm{D}^\top\mathbf{K}_\nu^{-1}(\mathbf{a}^\star)\mathbf{X}_\mathrm{D}. \tag{8.3}$$

This shows that (8.2) is the series connection of an inductor and a resistor.

8.2. Coupling. The structure of the model equations allows for two different representations and interpretations of the field-circuit coupling:

A. *source coupling*, in which the PDE model is represented in the circuit by a time-dependent current source $\mathbf{i}_\mathrm{D}$ (solving (8.2) for $\mathbf{i}_\mathrm{D}$), and vice versa the circuit excites the PDE-model by a time dependent voltage source, or,

B. *coupling with inductance*, where the inductive effect (of the PDE) is described by a series connection of a resistor with constant resistance $\mathbf{R}_\mathrm{D}$ and a time-dependent inductor with inductance $\mathbf{L}_\mathrm{D}$ (8.3); and the PDE model is excited by a time dependent voltage source.

These approaches are depicted in Fig. 8.2; compare with the semiconductor circuit coupling in Sect. 5. In the parameter coupling (B.), the inductance $\mathbf{L}_\mathrm{D}(\mathbf{a})$ is fitted according to the solution $\mathbf{a}(t)$ of the discrete PDE problem (8.1).

In a monolithic simulation, the two field-circuit representations are equivalent: one can interpret (8.3) as the Schur complement of (8.1–8.2). But in a weak coupling by a dynamic iteration scheme, both approaches behave differently. The coupling with inductance uses more physical knowledge than the source coupling. But the drawback

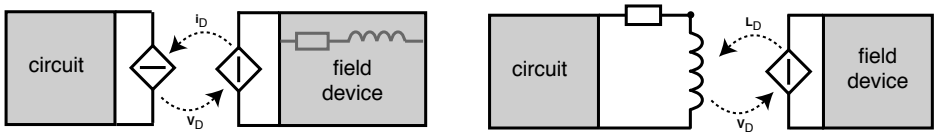

(a) Source coupling. (b) Coupling with inductance.

Figure 8.2: Coupling by current through the MQS device (a) and by an extracted inductance (b).

is the additional computational costs: the inductance matrices $\mathbf{L}_\mathrm{D}$ must be extracted by solving linear equations, cf. (8.3). For a given $\mathbf{v}_\mathrm{D}(t)$ the spatial discretization of the magnetostatic problem (8.1–8.2) yields an index-1 DAE. Additionally, we assume the coupled system to be of index-1, [6].
The abstract problem formulation is the same for source (A.) and parameter coupling (B.). Using the subscript c for the circuit and d for the Maxwell device, we obtain:

$$\begin{aligned} \dot{\mathbf{y}}_d &= \mathbf{f}_d(\mathbf{z}_d, \mathbf{z}_c), & \dot{\mathbf{y}}_c &= \mathbf{f}_c(\mathbf{y}_c, \mathbf{z}_c), \\ \mathbf{0} &= \mathbf{g}_d(\mathbf{y}_d, \mathbf{z}_d), & \mathbf{0} &= \mathbf{g}_c(\mathbf{y}_c, \mathbf{z}_c, \mathbf{z}_d), \end{aligned} \tag{8.4}$$

with regular $\partial \mathbf{g}_d / \partial \mathbf{z}_d$ and $\partial \mathbf{g}_c / \partial \mathbf{z}_c$ (due to the index-1 assumption for the circuit). The differential variables of the circuit and field equations are $\mathbf{y}_c := (\mathbf{q}, \mathbf{\Phi})$ and $\mathbf{y}_d := \mathbf{\Phi}_\mathrm{D}$, whereas the corresponding algebraic unknowns are $\mathbf{z}_c := (\mathbf{u}, \mathbf{i}_\mathrm{L}, \mathbf{i}_\mathrm{V})$ and $\mathbf{z}_d := (\mathbf{a}, \mathbf{i}_\mathrm{D}, \mathbf{v}_\mathrm{D}, \mathbf{L}_\mathrm{D})$. Thus both coupling variables $\mathbf{i}_\mathrm{D}$ and $\mathbf{L}_\mathrm{D}$ are components of $\mathbf{z}_d$.

9. Dynamic iteration for the field-circuit system. Independent of the coupling type (A) or (B), a Gauss-Seidel-type (device-first) dynamic iteration for the field-circuit system reads as splitting functions:

$$\mathbf{F} := \begin{bmatrix} \mathbf{f}_d(\mathbf{z}_d^{(k)}, \mathbf{z}_c^{(k-1)}) \\ \mathbf{f}_c(\mathbf{y}_c^{(k)}, \mathbf{z}_c^{(k)}) \end{bmatrix} \quad \text{and} \quad \mathbf{G} := \begin{bmatrix} \mathbf{g}_d(\mathbf{y}_d^{(k)}, \mathbf{z}_d^{(k)}) \\ \mathbf{g}_c(\mathbf{y}_c^{(k)}, \mathbf{z}_c^{(k)}, \mathbf{z}_d^{(k)}) \end{bmatrix}. \tag{9.1}$$

The only old iterate $\mathbf{z}_c^{(k-1)}$, i.e., the voltage drop defined by the circuit, enters a differential equation via the function $\mathbf{f}_d$. This setting is similar to the semiconductor-circuit problem (coupling with capacitances), see Lemma 6.2. We do not repeat the proof here, but conclude stability and convergence with rate $\mathcal{O}(\sqrt{H})$ by application of Corollary 3.7.

On the other hand it is not wise to reorder the computational sequence of the subproblems. Thus a Jacobi or — as given here — the Gauss-Seidel approach with

$$\tilde{\mathbf{F}} := \begin{bmatrix} \mathbf{f}_d(\mathbf{z}_d^{(k)}, \mathbf{z}_c^{(k)}) \\ \mathbf{f}_c(\mathbf{y}_c^{(k)}, \mathbf{z}_c^{(k)}) \end{bmatrix} \quad \text{and} \quad \tilde{\mathbf{G}} := \begin{bmatrix} \mathbf{g}_d(\mathbf{y}_d^{(k)}, \mathbf{z}_d^{(k)}) \\ \mathbf{g}_c(\mathbf{y}_c^{(k)}, \mathbf{z}_c^{(k)}, \mathbf{z}_d^{(k-1)}) \end{bmatrix} \tag{9.2}$$

will exhibit a non-vanishing contraction factor α, see equation (3.7). Consequently, convergence is not guaranteed by the theory above and divergence can occur similarly to the semiconductor example shown in Fig. 7.1a. Moreover, even in the case of convergence, we only can ensure a convergence rate of $\alpha_n + \mathcal{O}(H)$.[1] Thus, in the following numerical investigation, we employ the sequence as given in (9.1).

10. Numerical Results. In our application, the field model realizes a single-phase isolation transformer. Its configuration, see Fig 8.1b, is taken from the documentation of the software package `FEMM` (Finite Element Method Magnetics), [20].

[1] In the parameter coupling case (B.), the inductance enters the circuit effectively in a differential equation: the algebraic equation is just an evaluation, c.f. (4.1b) vs. (4.1c); Thus the convergence guarantee can be extended to both sequences (device-first and circuit-first).

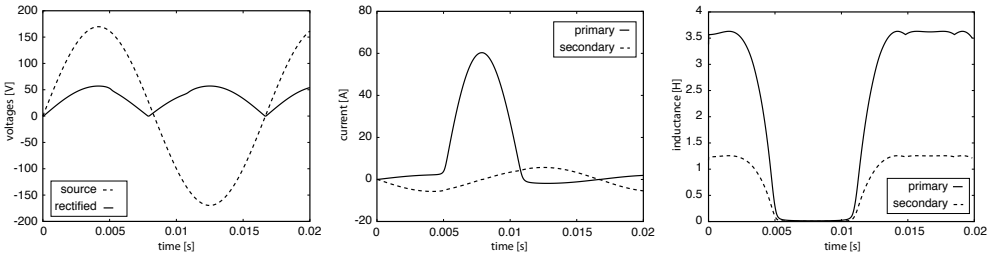

(a) Voltage drop at source (dashed line), and at the load resistance R_{load} (solid line).

(b) Currents through primary (solid) and secondary coil (dashed) of the transformer.

(c) Self-inductances of the primary (solid) and secondary coil (dashed) of the transformer.

Figure 10.1: Voltages, currents and inductance in the nonlinear transformer embedded in nonlinear rectifier circuit example Fig. 8.1.

The primary coil has 260 turns and the secondary coil has 90 tunrs. The reluctivity $\mathbf{M}_\nu$ is given by a highly nonlinear BH-curve taken from [11]. The attached rectifier circuit, Fig. 8.1a, is driven by a sinusoidal voltage source $v(t) = 160\sin(\omega t)\text{V}$ with $\omega = 2\pi \cdot 60\text{Hz}$. The diode currents are described by the lumped model

$$i = I_\text{s} \cdot \left(\exp\left(\frac{v}{V_\text{th}}\right) - 1\right) + G \cdot v; \quad \text{with} \quad G = 10^{-12}\frac{1}{\Omega}, \tag{10.1}$$

reverse saturation current $I_\text{s} = 10^{-9}\text{A}$ and thermal voltage $V_\text{th} = 2.5 \cdot 10^{-2}\text{V}$. The load resistor has a constant DC resistance of $R_\text{load} = 10\Omega$. The resistances of the coil windings are extracted from the FEMM model. This gives $\mathbf{R}_\text{D} = \text{diag}(0.44937, 0.061526)\Omega$.

The problem is simulated on the time interval from $t_0 = 0\text{s}$ until $t_e = 10^{-2}\text{s}$. For roughly a period of the applied signal, Fig. 10.1a–10.1c show voltages, currents and inductances. The dynamics of the plots in Fig. 10.1b–10.1c are mainly due to the nonlinear saturation of the transformer; the current peak (primary coil) reflects the inrush current in this start-up phase of the transformer.

All time-integrations have been carried out by the implicit Euler method with a fixed time step size $\Delta t = 10^{-5}\text{s}$. We applied both, the monolithic and the dynamic-iteration approach to the problem in Fig. 10.1. The monolithic simulation is used as a reference solution for the dynamic iteration approach. Thus we neglect the time-discretization error (introduced by Euler's methods) and focus only on the splitting error of the iteration scheme (8.4). For a single-phase transformer, the extracted inductance $\mathbf{L}_\text{D}(t)$ corresponds to a 2×2-matrix for each time-step t. We use spline interpolation to recover a waveform from the discrete inductances. The dynamic iteration has been run for various window sizes $H = 5 \cdot 10^{-5}\text{s}, \ldots, 10^{-2}\text{s}$ and up to 5 iterations per window. Fig. 10.2a shows the corresponding errors in the current through the first coil in dependence of those window sizes. We see — in accordance with the theoretic results of the previous section — that the error decreases with the time window size. In particular for small window sizes $H \approx \Delta t$ the first order accuracy of the implicit Euler would dominate and only higher order methods can yield an improvement here (independent of the number of window iterations).

The second convergence study, Fig. 10.2b, analyzes the number of iterations $k = 1, \ldots, 5$ per window. The plot shows the time-integrated error on the first time window $T = [0,\ H]$ with $H = 5 \cdot 10^{-3}\text{s}$, for varying k. It matches the expected first order for a simple coupled problem: we have shown that the contraction factor α vanishes and thus Corollary 3.7 is applicable.

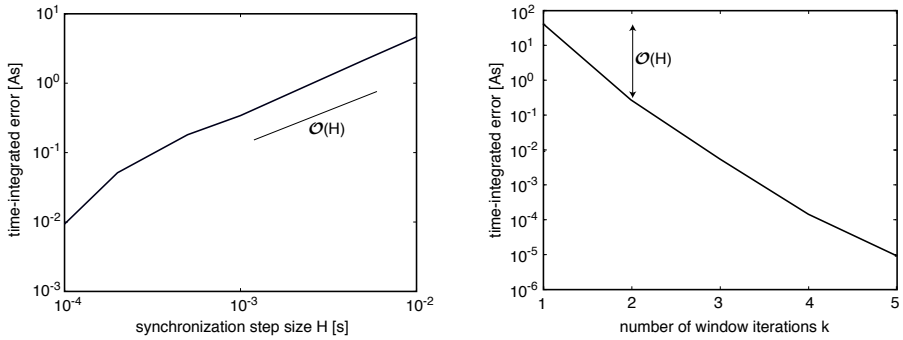

(a) The time-integrated error in the primary current on the full time interval in dependence of the synchronization step size H.

(b) Convergence of the primary current on the time window $[0,\ H]$ with $H = 5 \cdot 10^{-3}$ in dependence of the number of iterations.

Figure 10.2: Convergence study of the dynamic iteration scheme applied to the field-circuit coupled problem using the time step size $\Delta t = 10^{-5}$.

11. Conclusion. In this paper we have broadened the results of [3] to general index-1 DAEs. We have given a sufficient condition for convergence of dynamic iteration schemes applied to general index-1 DAEs. The error propagation for the windowing technique was examined and we have shown that under the given contractivity condition the dynamic iteration scheme is globally convergent and stable.

We have carried out a detailed analysis of important special cases of coupled index-1 problems. This included e.g. the simple coupling, where for a Gauss-Seidel dynamic iteration scheme the rate of convergence with respect to the time window size H can be higher than in the general case, namely $\mathcal{O}(H)$ instead of $\mathcal{O}(\sqrt{H})$. Often optimal modeling of the coupling interface is necessary to obtain the higher convergence rate. Especially in electrical engineering this can be of high interest since in applications incorporating radio frequency the chosen time window size usually is significantly smaller than one.

We have shown that the sequence in which different subsystems are simulated may be crucial to ensure convergence of the iteration scheme. Moreover, for the coupling of two subsystems we have shown that even if the contractivity condition is fulfilled for any sequence, the sequence of the subsystems influences the speed of convergence. As measure for this we have identified the Lipschitz constants.

We have applied our theoretical results to two different applications in electrical engineering; a coupled semiconductor-circuit system, as well as a coupled field-circuit system. For both applications we suggest a tailor-made modeling of the interface in order to ensure the best convergence of the applied iteration scheme. The simulations verify that our condition for convergence is sufficient. Moreover, the examples show, that without enhanced modeling of the interface and thus without fulfilling the contractivity condition, the iteration may be divergent. Thus the examples not only verify the theoretical results, but also show that in DAE-PDE coupling even for simple settings iteration schemes can suffer from divergence.

The identification of coupled systems consisting of more than two subsystems and coupling structures with a convergence rate higher than $\mathcal{O}(H)$ are subject to ongoing research. Furthermore, the consideration of the coupled field-semiconductor-circuit system is part of this ongoing research.

References.

[1] G. Alì, A. Bartel, and M. Günther. "Parabolic differential-algebraic models in electrical network design". In: *SIAM J Mult Model Sim* 4.3 (2005), pp. 813 –838.

[2] G. Alì et al. "A Convergent Iteration Scheme for Semiconductor/Circuit Coupled Problems". In: *Scientific Computing in Electrical Engineering SCEE 2010*. Ed. by B. Michielsen and J.-R. Poirier. To be published. Berlin: Springer, 2011.

[3] M. Arnold and M. Günther. "Preconditioned Dynamic Iteration for Coupled Differential-Algebraic Systems". In: *BIT* 41.1 (2001), pp. 1 –25.

[4] M. Arnold and A. Heckmann. "From Multibody Dynamics to Multidisciplinary Applications". In: *Multibody Dynamics. Computational Methods and Applications*. Ed. by J. García Orden, J. Goicolea, and J. Cuadrado. Springer-Verlag, 2007, pp. 273 –294.

[5] A. Bartel. *Partial Differential-Algebraic Models in Chip Design - Thermal and Semiconductor Problems*. Dissertation. Düsseldorf: VDI Verlag, 2004.

[6] A. Bartel, S. Baumanns, and S. Schöps. "Structural Analysis of Electrical Circuits Including Magnetoquasistatic Devices". In: *APNUM* (2011). To be published.

[7] A. Bossavit. "Whitney forms: a class of finite elements for three-dimensional computations in electromagnetism". In: *IEE Proceedings* 135.8 (1988), pp. 493–500.

[8] M. Brunk and A. Kværnø. "Positivity preserving discretization of time dependent semiconductor drift-diffusion equations". In: *APNUM* (2010). To be published.

[9] K. Burrage. *Parallel and sequential methods for ordinary differential equations*. Oxford: Oxford University Press, 1995.

[10] L. O. Chua and P. Y. Lin. *Computer aided analysis of electronic circuits*. 1st ed. Englewood Cliffs, NJ: Prentice-Hall, 1975.

[11] M. Clemens et al. "Decomposition and Regularization of Nonlinear Anisotropic Curl-Curl DAEs". In: *COMPEL* 30.6 (2011).

[12] F. Ebert. "On Partitioned Simulation of Electrical Circuits using Dynamic Iteration Methods". PhD thesis. Berlin: TU Berlin, 2008.

[13] D. Estévez Schwarz and C. Tischendorf. "Structural analysis of electric circuits and consequences for MNA". In: *Int J Circ Theor Appl* 28.2 (2000), pp. 131 –162.

[14] U. Feldmann and M. Günther. "CAD-based electric-circuit modeling in industry I: mathematical structure and index of network equations". In: *Surv Math Ind* 8.2 (1999), pp. 97 –129.

[15] K.-T. Grasser. "Mixed-Mode Device Simulation". PhD thesis. TU Wien, 1999.

[16] Z. Jackiewicz and M. Kwapisz. "Convergence of Waveform Relaxation Methods for Differential-Algebraic Systems". In: *SIAM J Numer Anal* 33.6 (1996), pp. 2303–2317.

[17] R. Kübler and W. Schiehlen. "Two Methods of Simulator Coupling". In: *Mathematical and Computer Modelling of Dynamical Systems: Methods, Tools and Applications in Engineering and Related Sciences* 6.2 (2000), pp. 93 –113.

[18] E. Lelarasmee. "The Waveform Relaxation Method for Time Domain Analysis of Large Scale Integrated Circuits: Theory and Applications". PhD thesis. EECS Department, University of California, Berkeley, 1982.

[19] L. D. Marini and P. Pietra. "New mixed finite element schemes for current continuity equations". In: *COMPEL* 9 (1990), pp. 257–268.

[20] D. Meeker. *Finite Element Method Magnetics User's Manual*. Version 4.2 (09Nov2010 Build). 2010.

[21] U. Miekkala and O. Nevanlinna. "Convergence of dynamic iteration methods for initial value problems". In: *SIAM J Sci Stat Comput* 8 (1987), pp. 459–482.

[22] M. Rathinam, Linda, and L. R. Petzold. "Dynamic Iteration Using Reduced Order Models: A Method For Simulation Of Large Scale Modular Systems". In: *SIAM J Numer Anal* 40 (2002), pp. 1446–1474.

[23] S. J. Salon. *Finite Element Analysis of Electrical Machines*. Kluwer, 1995.

[24] S. Schöps, H. De Gersem, and A. Bartel. "A Cosimulation Framework for Multirate Time-Integration of Field/Circuit Coupled Problems". In: *IEEE Trans Magn* 46.8 (2010), pp. 3233 –3236.

[25] M. Selva Soto and C. Tischendorf. “Numerical Analysis of DAEs from Coupled Circuit and Semiconductor Simulation”. In: *APNUM* 53.2–4 (2005), pp. 471–488.

[26] R. Stratton. “Diffusion of hot and cold electrons in semiconductor barriers”. In: *Phys Rev* 126.6 (1962), pp. 2002–2014.

[27] I. A. Tsukerman et al. “Coupled Field-Circuit Problems: Trends and Accomplishments”. In: *IEEE Trans Magn* 29.2 (1993), pp. 1701 –1704.

[28] P. K. Vijalapura, J. Strain, and S. Govindjee. “Fractional step methods for index-1 differential-algebraic equations”. In: *J Comput Phys* 203.1 (2005), pp. 305 –320.

[29] J. K. White et al. *Waveform Relaxation: Theory and Practice*. Tech. rep. UCB/ERL M85/65. Berkley: EECS Department, University of California, 1985.